The use of vanadium to enhance localised corrosion resistance in 18% chromium ferritic stainless steel.

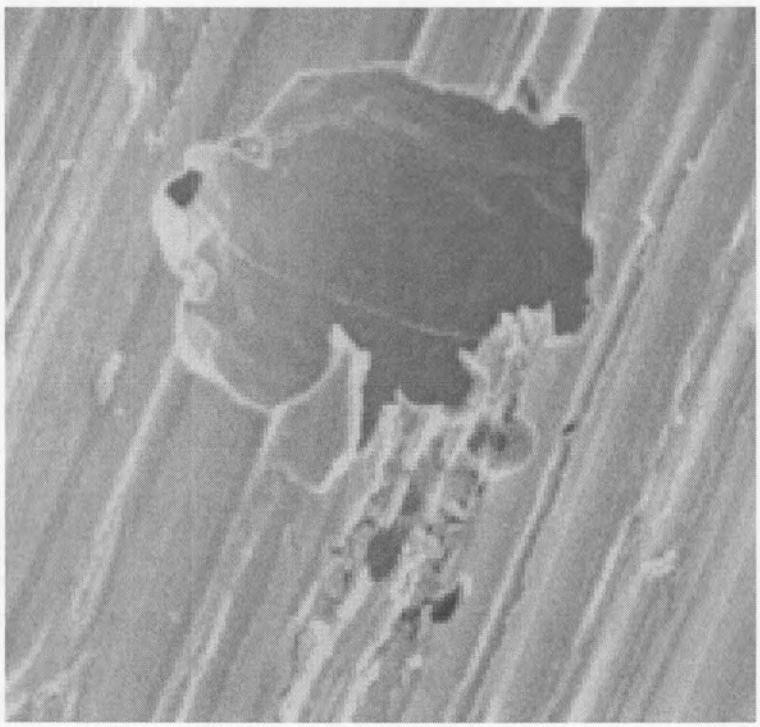

By
MH Ras

Submitted in fulfillment of a part of the requirements for the degree
Masters in Engineering

in the Faculty
Engineering, the Built environment and Information technology

University of Pretoria

2000

UNIVERSITEIT VAN PRETORIA
UNIVERSITY OF PRETORIA
YUNIBESITHI YA PRETORIA

The use of vanadium to enhance localised corrosion resistance in 18% chromium ferritic stainless steel.

deur
MH Ras

Leier:
Professor PC Pistorius

Departement Materiaalkunde en Metallurgiese Ingenieurswese

Magister in Ingenieurswese

Samevatting

In toepassings waar weerstand teen lokale korrosie verlang word word molibdeen bevattende roesvry stale gewoonlik gebruik as gevolg van hulle goeie weerstand teen lokale korrosie in aggressiewe omgewings. Daar is gevind dat vanadium toevoegings by ferritiese roesvry stale ook 'n positiewe uitwerking op die weerstand teen lokale korrosie het. In hierdie werk is vanadium en molibdeen toevoegings tot 18 % chroom ferritiese roevry stale direk vergelyk wat betref die uitwerking daarvan op die weerstand teen lokale korrosie. Die pit potensiale in 'n neutrale chloried oplossing is gebruik as die maatstaf om die weerstand teen lokale korrosie van die verskillende legerings te vergelyk en daar is aangetoon dat vanadium toevoegings dieselfde verhogings of self bietjie beter verhogings in die pitpotesiale gee as molibdeen, vir toevoegings tot by 4% (massa persentasie).

Daar is verder aangetoon in hierdie werk dat die meganismes, waarby vanadium en molibdeen die weerstand teen lokale korrosie verhoog, verskil. Die eksperimentele data bepaal vir die molibdeen bevattende materiale was in goeie ooreenstemming met ander werk gedoen in hierdie veld. Die verbeterende uitwerking van molibdeen op die pit korrosie weerstand van hierdie materiale kan toegeskryf word aan 'n verlaging in die oplos reaksietempo in die aktiewe oplosreaksie gebied deurdat daar 'n vereiking in molybdeen plaasvind op die metaal oppervlak wat besig is om op te los.

Die werk het getoon dat vanadium toevoegings nie 'n noemenswaardige uitwerking het op die kinetika van die oplos reaksie in die aktiewe oplos gebied nie. Die uitwerking van hierdie twee legerings elemente op die inisiërings stap van metastabiele putte is ondersoek, maar geen betekenisvolle verskille, wat wys dat die vanadium toevoegings 'n verbetering teweeg bring, kon gekry word nie. Dit word voorgestel dat vanadium betrokke is by die verandering van die die oplos kinetika van die sout lagie wat vorm tydens die groei fase van metastabiele putte. 'n Vertraging in die oplosreaksie tempo van oorblyfsels van die sout lagie kan lei tot die verlies van die verrykte oplossing binne in die metastabiele putjie wat dan sal lei tot herpassivering.

Summary

In applications where resistance to localised corrosion is required, stainless steel alloys containing molybdenum are generally used thanks to their superior resistance to localised attack in aggressive environments. For ferritic stainless steels, vanadium additions have been found to also have a beneficial effect on the resistance to localised corrosion. In this study vanadium and molybdenum were compared directly as alloying elements in 18% chromium ferritic stainless steel as far as their effect on increasing the resistance to localised corrosion is concerned. Pitting potentials in a neutral chloride solution were used as the criterion for qualifying resistance to localised corrosion and it was shown that vanadium gave similar or slightly higher pitting potentials at addition levels of up to 4% (weight percent).

It was subsequently found that the mechanism by which the molybdenum and the vanadium increase the resistance to localised corrosion, are not the same. The experimental data for the molybdenum containing alloys corresponded well with other work done in this field. The positive effect of molybdenum additions on the pitting resistance of these alloys could be explained through its effect in lowering the dissolution rate in the active dissolution region by enriching on the dissolving surface.

The vanadium additions to these alloys were shown not to have an effect on the active dissolution kinetics. The effect of these two alloying elements on the initiation of metastable pits were examined, but no meaningful advantage for the vanadium containing alloys over the rest could be found. It is suggested that vanadium play a role in changing the dissolution kinetics of the salt film, which forms during the growth of a metastable pit. A delayed dissolution of salt film remnants would lead to a loss of the enriched pit solution, which would cause the metastable pit to repassivate.

Keywords:
Localised corrosion, vanadium, molybdenum, pitting corrosion, 18% chromium ferritic stainless steel, metastable pitting, pit initiation, enriched pit solution, pit stability product, pitting resistance equivalent.

Acknowledgements

I would like to thank all the people who motivated and helped me through discussions and suggestions through the course of this project. I want to thank Professor Chris Pistorius in particular for his guidance, enthusiasm and time. I am grateful to Mintek who made this project possible and to Mr Bob Paton for his guidance. I would like to thank the people at the Department of Material Science and Metallurgical Engineering of the University of Pretoria, especially Mr M. Prozzi, Ms M. Sephton, Mr N Bormann and Prof. G.T. van Rooyen. Also Dr. P.G.H. Pistorius, Mr R. Bezuidenhout and Mr B. Benadi not with the University any more. I would like to thank the Physical Metallurgy division at Mintek as well as Division of Electron Microscopy at the University of Pretoria for making their facilities and expertise available to me. I am grateful for the support from the people close to me.

Table of Contents

Appendices

1. Background

Ferritic stainless steels have found important applications in environments where corrosion resistance is of primary interest. This group of alloys has the advantages over their austenitic counterparts in that they do not require nickel to stabilize the austenite phase and therefore have the possibility of lower alloy cost. It is also thought that this group of stainless steels has a superior resistance to stress corrosion cracking in chloride environments compared to there austenitic counterparts [1]. With the advances in the manufacturing of cleaner steel (argon-oxygen decarburisation [AOD] and vacuum-oxygen decarburisation [VOD]), leading to improved resistance to pitting and crevice corrosion [2], ferritic stainless steels could be a more attractive alternative.

One of the major problems with the use of stainless steels in highly corrosive environments is the well-known phenomenon of localised corrosion. Pitting corrosion, crevice corrosion, intergranular corrosion, and stress corrosion cracking are all included in this type of attack and have been the cause of concern in many applications of stainless steel. This work takes a look at pitting corrosion in order to qualify the resistance to localised corrosion.

Pitting is the rapid corrosion attack at small areas, which leads to relatively fast penetration of normally passive materials and subsequent failure of pipes, thin walled reactor vessels, etc. This is most commonly found in stainless alloys in neutral-to-acid solutions containing chloride or chlorine containing ions as is frequently found in marine and chemical process environments [3].

1.1 Factors influencing pitting corrosion

It is believed that localised corrosion is generally associated with heterogeneities in the metal and/or the environment [4]. Environment (solution severity), alloy composition, surface treatment, microstructure and other metallurgical processes such as galvanic interactions all seem to influence the pitting behavior of a material.

Some alloying elements have been found to influence the resistance to localised corrosion. It has been shown that an increase in chromium content in stainless steels leads to an increase in pitting resistance [3,5,6]. Molybdenum, vanadium, tungsten, rhenium, nickel and nitrogen have also been named as alloying elements generally increasing the pitting resistance [4]. Other oxidisable elements such as silicon may also improve resistance through entering the passive film [6]. Elements like sulphur, carbon and manganese have usually been found to be detrimental to the pitting resistance [3].

Some environmental factors are generally associated with promoting localised corrosion. These include the presence of aggressive anions, the neutral to acidic pH of the surrounding solution and elevated temperatures. An increase in aggressive ion concentration, a decrease in pH and an increase in temperature usually favour localised attack [3]. Galvele tabulated a list of aggressive anions including the halide anions Cl^-, Br^- and I^- as well as others such as nitrate, sulphate and perchlorate all of which could cause pitting on different metals [4]. In practice localised corrosion is mostly associated with environments containing chloride ions. The chloride ion is said to destabilise the passive film locally [6]. Some anions also act as inhibitors of pitting.

For stainless steel some of the weaker acid salts act as inhibitors [4]. Physical crevices on equipment generally increase the chances for localised attack. Where dissimilar metals are in contact, galvanic coupling may accelerate localised attack [3]. Surface characteristics and microstructure, which can have a substantial influence on the localised corrosion resistance, are both partially determined by the metallurgical processing of the material [6]. Phase equilibria, segregation, inclusions and precipitates can all play a role during localised corrosion.

1.2 Definitions

The **pitting potential** is defined as that potential below which no stable growing pit forms. In practice this theoretical value is difficult to determine. The experimental procedure, including factors like the type of test (potentiostatic, potentiodynamic, etc.) and the surface condition, has a strong influence on the measured values [6].

The **induction time** is defined as the time it takes for pitting to be detected from the time a material is placed in a certain environment [4].

The **repassivation potential** is found when potential scan is reversed after the material has started to pit during a potentiodynamic scan test and is defined as the potential where the current reaches the same current as on the positive scan at a specific potential. The measured potential is strongly dependent on the experimental procedure – specifically how much the sample is pitted [6].

The **critical pitting temperature** (CPT) is defined as a temperature where there is a noticeable difference in the resistance to pitting corrosion. It has been defined as the temperature where there is a sudden decrease in pitting potential when determining the pitting potential at increasing temperatures. Again this value depends on test conditions.

The **Pitting Resistance Equivalent** (PRE) is an expression used to compare different stainless steels as far as their resistance to localised corrosion is concerned by taking the alloying content into consideration. The PRE is proportional to the chromium content. The effect of other alloying elements on pitting resistance is then determined relative to that of chromium and they are given a corresponding coefficient in the expression. These expressions assume a linear relationship between the alloy content and the measured effect such as pitting potential or CPT. Different investigators have found different coefficients for elements such as molybdenum and nitrogen. Alfonsson and Qvarfort [7] tested a few such expressions found in literature, against CPT values which they determined experimentally. They performed potentiodynamic scans in 1M NaCl at varying temperatures for some commercial austenitic stainless steels and fitted the expressions through the data determining a standard deviation. They found acceptable linearity between the CPT and all the PRE expressions examined and concluded that the PRE expressions are merely rough estimates of the pitting resistance of alloys and that small differences in coefficients have no real importance. The coefficient for Mo in all the expressions examined were either 3 or 3.3 [7]. Bavay [5] found a linear relationship between the minimum pitting potentials (the lowest measured value of a number of tests) of some super ferritic stainless steels in NaCl solution and the expression:

$$PRE = (\%Cr) + 3.3\times(\%Mo) \quad \ldots\ldots\ldots\ldots\ldots (1)$$

It was postulated that in ferritic stainless steels the coefficient for molybdenum is a little lower and that for nitrogen there is of course no factor because it has such a low solid solubility in the body-centered-cubic-structure and because it promotes nitride formation which has a negative effect on corrosion resistance[2]. By plotting experimentally determined breakdown potentials against PRE expressions and varying the weighting factor for molybdenum an optimum PRE expression was determined which gave the best linear fit. The optimum coefficient for molybdenum content in these ferritic stainless steels was determined to be 2.5.

1.3 Electrochemical measurement

Tests to evaluate the performance of alloys as far as resistance to localised corrosion is concerned can generally be divided into two groups: exposure tests and accelerated tests. Accelerated tests are again divided into electrochemical and chemical tests. The chemical or immersion tests have the advantage of being fairly simple in the respect that they do not require electronic instrumentation [8].

With immersion tests a series of exposures of differring severity is necessary to evaluate and compare the pitting resistance of a set of alloys and this can be very time consuming. With electrochemical testing quantification of the pitting resistance and differentiation based on small differences is possible in a short time [9].

Electrochemical tests include [8]:

- potentiokinetic tests where the current is determined as a function of the potential ($I = f(E)$),
- potentiostatic tests where the current is determined as a function of time at a given potential ($I = f(t)$),
- galvanokinetic tests where the potential is determined as a function of the current ($E = f(I)$),
- and galvanostatic tests where the potential is determined as a function of time at given current($E = f(t)$).

Potentiodynamic scanning at a constant temperature is an attractive option for various reasons. It is a fairly simple test to perform. In principle, only one test is required to determine a pitting threshold potential, although the pitting potential is subject to statistical variation, and in practice more than one test is necessary to determine a confidence interval. This test is widely used and a large body of data is available on the pitting potentials of various alloys. Good correlation was found for 18-20% Cr, 10-25% Ni and 2-6% Mo alloys between pitting potentials determined with potentiodynamic scans performed in 3.56% NaCl and critical pitting temperatures determined by stepping the temperature up every 24 hours in 10% $FeCl_3$ solution [28].

When a sharp increase in the anodic current occurs that is irreversible (current does not return to its passive values) the sample is considered to be pitted [6]. Many investigators prefer to use a certain critical current density magnitude to define the pitting potential rather then the change in slope on the curve, which is often obscured by electrochemical or instrumental noise.

A critical scanning rate exists where the pitting potential measured is a minimum. Higher scanning rates lead to an increase in measured pitting potential due to the

induction time effect and lower scanning rate lead to increased measured pitting potentials because the passive layer is modified during the scanning and becomes more resistant to pitting [6].

During the electrochemical determination of the pitting potential, low frequency electrochemical noise has been observed in the measured current or potential. It is now generally believed to be due to the formation and repassivation of metastable pits at potentials below the pitting potential. For example, by performing very sensitive measurements during electrochemical tests and subsequent scanning electron microscopy on the samples, Williams *et al.* found exactly the same number of pits as the electrochemical events observed during the test. There was also good correlation between the size of the pits calculated from the charge and the actual observed size of the pits [10].

1.4 Effect of molybdenum

Molybdenum is commonly added to stainless steel alloys to increase the resistance to localised corrosion. The positive effect of molybdenum on the localised corrosion resistance of ferritic stainless steels has long since been shown using various tests like the electrochemical determination of critical pitting temperature [11] and pitting potentials [12,13,14,27]. Lizlovs and Bond showed that Mo decreases the critical current density necessary for passivation of ferritic stainless steels in 0.1N HCl [12]. Some investigators also indicated a synergistic effect between Mo and Cr in decreasing the critical current density and shifting the pitting potential to more anodic potentials [2,13]. Linear relationships were found between %Mo and pitting potential at 25°C [13] and 35°C [2].

1.5 Mechanisms

When considering mechanisms, it is useful to distinguish between three different phases of pitting namely initiation, metastable growth and stable growth. The mechanisms involved in initiation include the localised breakdown of passivity and the establishment of a sheltered anodic area. The mechanisms involved in the growth phases include the reactions and factors necessary to sustain the accelerated anodic reaction inside the sheltered area.

Initiation

It was found that pit initiation is mostly related to microscopic features in the metal surface [4]. Dowling *et al.* stated that galvanic coupling or crevice geometry at the metal-inclusion interface is almost always involved in the initiation of pits [2]. Sulphide inclusions are commonly accepted to be the greatest contributor in this regard [15,6].

As far as the actual initiation events are concerned, a few mechanisms have been described. According to the ion migration mechanism aggressive anions migrate into passive film and change the properties of the film making it susceptible to breakdown. Film contamination by aggressive anions was however also detected below pitting potential, showing this not to be the determining step [4]. Another suggested

mechanism is the mechanical breakdown of the passive film, which was suggested to be probable but not sufficient in itself to initiate pitting [4]. There are also mechanisms based on the partial or complete dissolution of manganese sulphides leading to pit initiation by exposing metal and creating local acidification and enrichment of sulphur species, which prevent the metal from repassivating [6].

Isaacs and Newman established that the initiation of a pit requires a sudden pit current of a magnitude in the region of 1μA [16]. This current is necessary to dissolve enough metal to create a pit large enough to sustain the anodic reaction. This current has to be supplied by a cathode without a too large drop in potential, which would lead to immediate repassivation of the pit. It is believed that this current is initially supplied by the capacitance over the passive layer.

Isaacs and Ishikawa experimentally examined the electrical response of a single pit using a vibrating electrode setup [17]. From this electrical response they derived an electrical equivalent that gave electrical responses closely resembling that which they measured. This equivalent circuit emphasised the importance of the capacitance component of the passive surface during rapid changes in the potential, following either change in applied current or pit initiation. They suggested that the stabilising stage after initiation is dependent on the characteristics of the capacitance of the surrounding passive area and not on the rate of oxygen reduction reaction. This dependence on the capacitance characteristics would also have a strong influence on the distribution of the pits.

Recently very small electrochemical events have been measured using microelectrodes and a very sensitive setup; these small events are believed to be related to pit initiation [18]. Two forms of current events could be identified: Slow rise and fast decay current events typical of metastable pit growth, as well as much smaller current spikes which were found to precede most metastable events or to stand alone. These are believed to be initiation events. The number of initiation events found on a stainless steel sample was seen to be finite. This seems to confirm that initiation takes place on inclusions such as sulphides in stainless steel. A model was proposed according to which chloride enters into the passive film to form metal chlorides causing stresses in film leading to rupture. It is believed that, if following film rupture the solution adjacent to the exposed metal surface is concentrated enough metastable pitting will occur, but if the chlorides were washed out straight away immediate passivation would follow. Some confirmation of this model was found in events where some growth had taken place which ended in a gradual decrease in the current and not the abrupt drop, which is associated with rapture of pit cover (see below). It was stated that as with metastable pitting, the geometry of the pit embryo plays a major role in determining further propagation.

Maintaining the anodic reaction

Maintaining the anodic reaction inside the pit is seen by many to be the biggest challenge for a small pit to grow into a stable growing pit.

A general mechanism for pit stabilisation was suggested by Galvele [19]. He formulated a model describing pitting based on transport processes in which he relates pit initiation to critical pH formation inside occlusions, which are said to form

naturally in the passive film through a dynamically process of rupturing and healing. In this model the pitting potential is related to the corrosion potential of the metal in the pit solution where the production and the consumption of protons are at steady state [4]. Galvele expressed the ion concentrations as functions of the product of the depth and the current density in a unidirectional pit (this product is referred to as the stability product). This enabled him to quantitatively explain the effects of pH, buffer solution and inhibitors on the pitting potential and to show that the acidification processes took place at pit initiation (in pits that are equivalent in size to cracks in the passive film). A critical stability product will lead to pitting and needs to be sustained in order to sustain pitting. The repassivation potential and its dependence on pit depth are also explained through this mechanism. The role of alloying elements is described as modifying the corrosion potential inside the pit solution [19]. A pit will repassivate once the concentration of aggressive ions in the solution inside the pit falls below a critical concentration. If the rate by which ions leave the pit through diffusion is greater than the rate by which new ions enter the solution thorough dissolution of the metal surface and the migration of anions into the pit to maintain charge balance, this would be the case [20]. This model explains many of the phenomena around pitting, but it partly relies on the assumption that the first pits initiate at the pitting potential. It does not explain metastable pitting which was later discovered to initiate at potentials far below the pitting potential.

Pistorius and Burstein showed that for type 304 stainless steel in 1M chloride solution the critical stability product is around 3mA/cm [20]. This value was determined by assuming open hemispherical pits and calculating the necessary current density (i) at a given diffusion barrier (assumed to be the pit radius x) in order to sustain a sufficiently concentrated solution inside the pit to maintain the anodic reaction. They experimentally determined xi values for some 200 metastable pits in a 304 stainless steel and found that with not one was the minimum required xi value of 3mA/cm ever reached. This was shown to be true for the initial growth of stable pits as well. It was also shown that the initial growth of stable pits was similar to the growth of metastable pits. It was concluded that all stable pits start out by growing in metastable fashion before becoming stable.

Many investigators suggested that the opening of a pit is partially covered by a thin film during its early development. This film is believed to be the passive film, which is still partly intact [21,20,6]. Isaacs and Kissel showed the dependence of the propagation of active pits on the surface properties, which determine the passive layer properties [21]. They concluded that the number of active pits was more dependent on passive film properties than on initiation factors. The possible collapse of the thin cap, partly covering pits, could lead to passivation of the pit due to the loss of the sheltered anodic area. The cover acts as another diffusion barrier, which helps maintain the aggressive solution inside the pit where the physical geometry is not enough of a barrier [20]. If the radius of the pit is greater than some critical value the pit will remain active even if it is open. Pistorius and Burstein concluded that the pit cover was essential in sustaining the metastable pit growth phase. Without the cover the metastable pits would not be able to survive and grow to reach the necessary stability product [20].

Diffusion control

Isaacs showed through a series of artificial pit experiments that a compact layer must exist inside the dissolving pit with this resistive layer having an ohmic resistance that depends on its thickness [22]. The measured properties of the film led him to believe that it is a metal chloride layer with a given solubility product. He came to the conclusion that a change in potential would only change the thickness of the film and not the reaction rate which is predominantly dependant on the diffusion rate away from the film. Work was done examining the effect of sulphate additions to a chloride solution on the pitting characteristics [23]. It is believed that the sulphate anions limit the solubility of the salt film, thereby decreasing the reaction rate. This work confirmed that for stainless steel in chloride solutions, metastable pitting as well as stable pitting likely takes place under diffusion control with a salt film on the dissolving surface.

Isaacs and Newman showed that a substantial supersaturation is necessary for salt film precipitation [16]. The applied current must be at least 1.3 times the magnitude of the diffusion-controlled value before salt film will precipitate and limit the current [16].

For such diffusion controlled growth it was shown that current density (i) varies inversely with the square root of the time by deriving an expression theoretically which was confirmed experimentally [22]. Tester and Isaacs again showed that the rate of reaction (dissolution) was independent of the applied potential [24]. When taking into account the changes made to the viscosity by an increase in the concentration of the pit solution good correlation was found with the mass transfer model.

Pistorius and Burstein illustrated the effect of potential on a single pit by initiating a metastable pit at 700 mV (SCE) and then scanning the potential down to around 400 mV where the metastable pit repassivated [20]. They calculated the current density and showed that a change in potential had no effect on the current density, thus confirming diffusion control. For stable pit growth it was shown that the pits grow in two regimes. The first is with the current proportional to the square of the time (constant current density). Metastable pits were generally found to grow in this mode. The measured current transients grew in a stepwise fashion with sharp increases in the current, separated by regions where the current stayed fairly constant. The overall increase in current could be approximated to be proportional to the square of the time. The repassivation of the metastable pit is always preceded by a sharp increase in current. It is believed these sharp increments in current are associated with ruptures in the film partially covering the pit, leading to increases in the diffusion rate, leading to transient increases in the dissolution rate [20].

After about 3 seconds of metastable growth there is a transition from growth at constant current density to growth at decreasing current density with time. During the second phase the pit grows with an approximately constant stability product [20]. Newman and Franz examined stable growing pits in 304 stainless steel in 1M NaCl and concluded that the growth basically followed Ohm's law and that the current was approximately proportional to the square root of the time [25]. However, this functional relationship could equally arise during diffusion-controlled growth.

Effect of initiation site geometry

Pistorius and Burstein described the potential dependence of pitting in terms of the geometry of pit initiation sites [20]. They showed that metastable pits which grew to become stable, initially grew with higher current densities. They postulated that this was possible because the initiation site geometry for these pits was more open and allowed a bigger hole in the film covering the pit, which allowed faster diffusion and thus a faster dissolution rate. These more open sites are however only susceptible to initiation at higher potentials because a higher active dissolution rate is necessary to balance out the higher diffusion rate and prevent loss of pit electrolyte. This role played by the original initiation site geometry was again emphasised in work examining the effect of chloride content of the solution on the metastable pitting of stainless steel [26]. It was shown that a decrease in chloride content of the solution led to a decrease in the frequency of metastable pit formation.

Role of molybdenum

Early work already suggested that molybdenum decreased the critical current density for passivation of chromium stainless steels in acid solutions [12]. Performing electrochemical tests in 1 M HCl Galvele *et al.* found that an increase in molybdenum content in 18% chromium ferritic stainless steel led to a decrease in the current density in the active dissolution region [27]. They examined actual pits grown in 1N NaCl and 1 M HCl and calculated the mean current density inside these pits to be about 0.5 A/cm^2. They found that all the pits observed were hemispherical and that a thin oxide layer covered most. Performing AES analyses (Auger electron spectroscopy) on the films formed inside the pits in the 1 M HCl solution, they showed that there is no enrichment of molybdenum in the films [27].

It was also shown that molybdenum had a stronger positive effect on the crevice resistance than on the pitting resistance [28]. This also suggests that molybdenum is more involved in restricting growth rather than initiation.

Galvele *et al.* performed Auger electron spectroscopy (AES) analyses on the passive surfaces formed during polarisation in the pseudo-passive zone, which they determined for the 18% chrome ferritic stainless steels containing different amounts of molybdenum [27]. They found no enrichment of molybdenum in the films which formed. Olefjord and Elfstrom (1982) also used surface analyses (electron spectroscopy for chemical analysis, XPS) to study the surface composition of molybdenum containing austenitic stainless steels after polarisation in the active and passive regions. Their equipment allowed them to treat the samples in an electrochemical cell (0.1M HCl + 0.4M NaCl solution) and then to transfer the samples to the electron spectroscopy chamber with the minimum of oxidation so that they were able to analyse the active surface after polarisation. They found that chromium, molybdenum and nickel were enriched on the metal surface during active dissolution. They suggested that these elements enrich on the surface due to selective iron dissolution and that this leads to passivation [29].

Comparing two austenitic stainless steel alloys, one containing 2.7% Mo, Newman and Franz showed that the molybdenum addition had no effect on the first few seconds of repassivation in the sulphuric acid [30]. This gives reason to believe that Mo

does not play a role in the early growth of the passive film. It did however decrease the active current density on a newly scratched surface. They calculated that the effect was already evident after the dissolution of only 5 atomic layers of metal which relates to a molybdenum concentration of 8 atomic %. They concluded that molybdenum acts on a sub-monolayer level decreasing the active dissolution rate of stainless steel.

In further work Newman showed that the effect of molybdenum on lowering the active current density comes into play before enough molybdenum is dissolved to form a MoO_2 monolayer [31]. This was shown in a HCl solution when 1.5% molybdenum already showed an inhibitive effect after only 1 to 2 atomic layers of alloy have been dissolved. He suggested that molybdenum in its elemental form must be responsible for lowering the current density by enriching on surface kinks or step sites in the active state.

Newman made use of "lead in pencil" electrodes to simulate single pits. It was found that two alloys, one with 2.7% molybdenum and one without molybdenum gave similar diffusion-controlled current densities in the region of 90 mA/cm^2 for a 1mm deep pit [32]. It was therefore said that the molybdenum has a negligible effect on the solubility of $CrCl_3$. Further data that was generated through this experiment was a current density – potential relationship describing the active dissolution kinetics inside the pit. The solution resistance was measured for the pit solution and adjusting the data for the IR drop at higher potentials gave an anodic 'Tafel slope' of around 80 mV. The 2.7% molybdenum caused the 'Tafel line' to shift by about 60 mV in the anodic direction.

Newman and Isaacs performed artificial pit experiments on a Fe-19Cr-10Ni experimental alloy and a commercial type 304L stainless steel in 1M NaCl at 25°C [33]. They stabilised diffusion controlled dissolution at 200 mV (SCE) before stepping the potential down to different potentials in the range –200 to –350 mV and measuring the current density against time. The metal surface inside the artificial pit is then exposed to a decreasing concentration of pit electrolyte, which can be calculated under the assumptions of a constant diffusivity and a negligible new dissolution rate. In this way they could determine the current density – concentration (of Fe^{2+}, $Cr^{3+}$and Ni^{2+}) relationship for the alloy and they proposed that there are usually two or more diffusion-coupled steady states of which one is usually stable.

Isaacs and Kaneko summarised the factors leading to passivation of pits as higher rates of mass transfer, lower active dissolution and higher critical concentrations for repassivation [34]. They also showed that molybdenum decreased the active dissolution rate inside an artificial pit for chloride bulk solutions and stated that molybdenum would therefore directly promote pitting resistance. The molybdenum however caused only a small decrease in active dissolution rate for bromide bulk solutions and this correlates with the lack of improvement in pitting resistance in bromide solutions brought about by molybdenum additions.

Laycock and Newman proposed a model where metastable pits are under mixed activation/ohmic control at lower potentials and under diffusion control at higher potentials with a salt film present in the pit [35]. The potential dependence then comes into play as a transition potential (E_T) above which a salt film is formed and diffusion

control dominates. This transition potential was shown to increase linearly with the log of the limiting current density. The differences in measured E_T values for different alloys were shown to correlate well with the differences in pitting potentials. It is proposed that all pits initially grow metastably covered with a film over the pit mouth to sustain the pit electrolyte. If the pit then does not have a salt film when the cover ruptures, it would become passive. The transition potential (E_T) is then described as the minimum potential where a salt film can be maintained. E_T was found to be moved to higher potentials by molybdenum due to its role in decreasing the anodic dissolution in the pit.

Laycock *et al.* also found a relationship between the critical pitting temperature (CPT) and the role which the salt film played within metastable pits [36]. The CPT was related to the transition from metastable pits to stable pits.

By referring to this mechanism involving the transition potential, Newman was able to explain the effect of molybdenum in increasing the pitting potential of austenitic stainless steels in chloride solutions while having almost no effect on the pitting potential in bromide solutions [37].

Other suggested models for molybdenum

Sugimoto and Sawada (1976) suggested that a small amount of MoO_4^{2-} ions suppressed pit initiation and growth for an austenitic stainless steel in neutral NaCl solution [38].

Wanklyn (1981) showed that Mo^{III} in solution had no inhibition effect on the corrosion of stainless steel. He concluded that Mo passes directly from metal to a passive film (probably consisting of insoluble Mo^{IV} oxide) which does limit the corrosion [39].

Qvarfort used scanning electron microscopy and electron dispersive X-ray spectroscopy to study pits in a 6 Mo stainless steel, (254 SMO) formed in 1M NaCl solution, and analyze their walls. He concluded that a molybdenum rich, thick porous, oxide layer, which is precipitated at early stages of pit growth, decreases the corrosion rate favouring repassivation while the material directly under this layer is depleted of molybdenum [40].

1.6 Effect of vanadium

It has been shown that an increase in vanadium content leads to an increase in the pitting potential of 18% chromium ferritic stainless steels [41,42].

Brookes and Graham examined the effect of Mo, V and W additions to 18% chromium stainless steels on the corrosion characteristics in 0.1M H_2SO_4 (pH 0.6) [42]. They found that all three elements lowered the dissolution rate in the active range but with molybdenum having a far greater effect. Mo and V also seemed to cause the primary passivation potential to shift to lower anodic potentials while W caused a shift to higher anodic potentials. They showed that Mo and V additions increased the pitting potential in 0.1M NaCl solution while W decreased it.

Goetz *et al.* showed that increases in V, Mo, W, Si content lead to an increase in pitting potential of 13Cr stainless steel in 1M HCl and suppressed pitting completely in a 24Cr stainless alloy [43]. Using Auger Electron Spectroscopy (AES) depth profiling they found that vanadium was not measurably enriched at the surface during active dissolution in 1M HCl.

Tjong showed that V additions to 17Cr stainless steels increased the pitting potentials in 5%HCl solution. He also suggests a synergistic effect between V and Cr as far as increasing pitting corrosion resistance is concerned [44].

Premachandra and Paton found that vanadium additions to 18Cr stainless steel alloys at the 1.5% level gave the same pitting potential values in 1M NaCl at 25°C as a type 444 (~2%Mo) commercial stainless steel [45].

Scheers and Paton [46] and Paton *et al.* [47] used galvanokinetic tests and immersion tests to make comparisons between the crevice corrosion resistance of commercial types 304, 316L and 444 stainless steels and two 18% chromium stainless steels containing 2 and 4% vanadium respectively. They found the 4% vanadium-containing alloy to be the most resistant in 3.5% NaCl in showing the highest transition temperatures under crevice and pitting conditions (CCT and CPT).

Apart from the improvement in the localised corrosion resistance by vanadium additions to 18 Cr ferritics stainless steels, the vanadium bearing ferritics seem to perform well in other areas as well. Increases in hardness, proof stress and fracture toughness and a decrease in ductile to brittle transition temperature were found with an increase in the vanadium content of 18Cr ferritic stainless steel from 0 to 4%. With the introduction of titanium stabilisation, good formability properties were also found [48].

1.7 Aim of work

The work reported here is concerned with the evaluation of vanadium as an alloying element in 18% chromium ferritic stainless steel to enhance localised pitting resistance. Molybdenum is generally used in this application and therefore one of the aims is to compare the effect of vanadium additions directly with molybdenum additions. Another aim is then to compare the mechanistic role played by vanadium with that of molybdenum and to try to establish a model for the effect of vanadium.

2. Experimental work

2.1 Experimental Alloys

The experimental alloys were based on an 18% chromium ferritic stainless steel (type 430). Alloys with similar amounts of respectively vanadium and molybdenum were prepared in order to make direct comparisons possible. These were a base alloy (type 430) and alloys with vanadium or molybdenum additions at 1, 2 and 4 % levels.

2.1.1 Manufacturing

The experimental alloys for this work were manufactured at Mintek (Randburg, South Africa). The alloys were melted in a vacuum induction furnace to keep the carbon and nitrogen contents low. 5-kg ingots were cast and cooled in the vacuum of the furnace. Table 2-1 gives the main alloy contents of the experimental alloys. A full analytical analysis is included in Appendix A. Surface grinding was done to remove surface defects. The ingots were then homogenised at 1150°C for 2 hours and subsequently hot rolled down to 4.5 mm plate with the finishing temperature in the region of 820°C. The hot rolling involved a reduction of about 3 mm with each pass and reheating of the plate after every four passes. It was then water quenched before it was annealed for 30 minutes at 950°C and water quenched again. Cold rolling took the plate thickness down to 1mm. It was again annealed and quenched as mentioned above. After the both hot and cold rolling the material was pickled in 10% H_2SO_4 at 70°C.

Table 2-1: Alloy content of experimental 18Cr alloy steels (mass percentage)

Material	C	N_2	Mo	V	Cr
Base	0.021	0.023	0.025	<0.005	17.7
1 V	0.022	0.022	0.03	0.89	18.1
2 V	0.024	0.023	0.03	1.88	18.0
4 V	0.027	0.025	0.03	3.77	18.0
1 Mo	0.021	0.025	0.92	0.10	18.0
2 Mo	0.020	0.021	1.93	0.009	18.0
4 Mo	0.023	0.021	3.80	0.009	17.7

2.1.2 Light microscopy

The microstructures of the different alloys are shown in Figure 2-1. These microstructures were revealed by setting pieces of the 1-mm plate into resin, polishing down to 1-µm finish and electro-etching. The etching was performed in a 30% HNO_3 solution at room temperature at 0.2 A/cm^2 for 120 min. The fine recrystalised ferrite structure is clearly evident for all the alloys with ASTM grain size numbers between 6 and 10. Figure 2-2 compares the carbide structures for the base, the molybdenum containing and the vanadium containing alloys. These structures were revealed by again setting and polishing the 1-mm plate down to a 1-µm finish and etching in oxalic acid at a potential of 6 V for 8 to 10 seconds. It can be seen that the base metal, like all the molybdenum containing alloys, contains carbide stringers whereas all the vanadium containing alloys have a finely dispersed carbide structure.

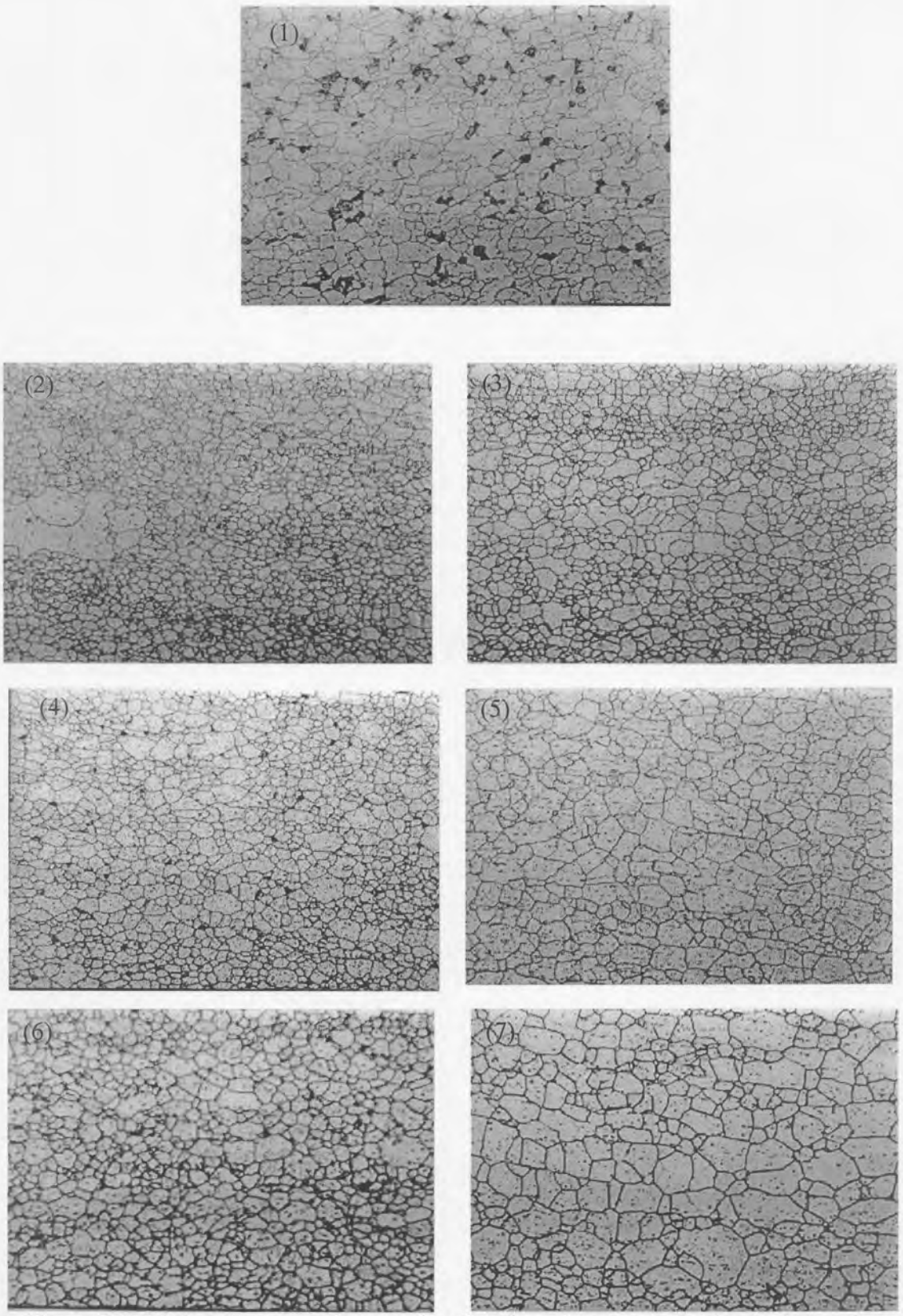

Figure 2-1: Light microscope images showing the microstructure of experimental alloys (100×). (1) Base, (2) 1 V, (3) 1 Mo, (4) 2 V, (5) 2 Mo, (6) 4 V, (7) 4 Mo

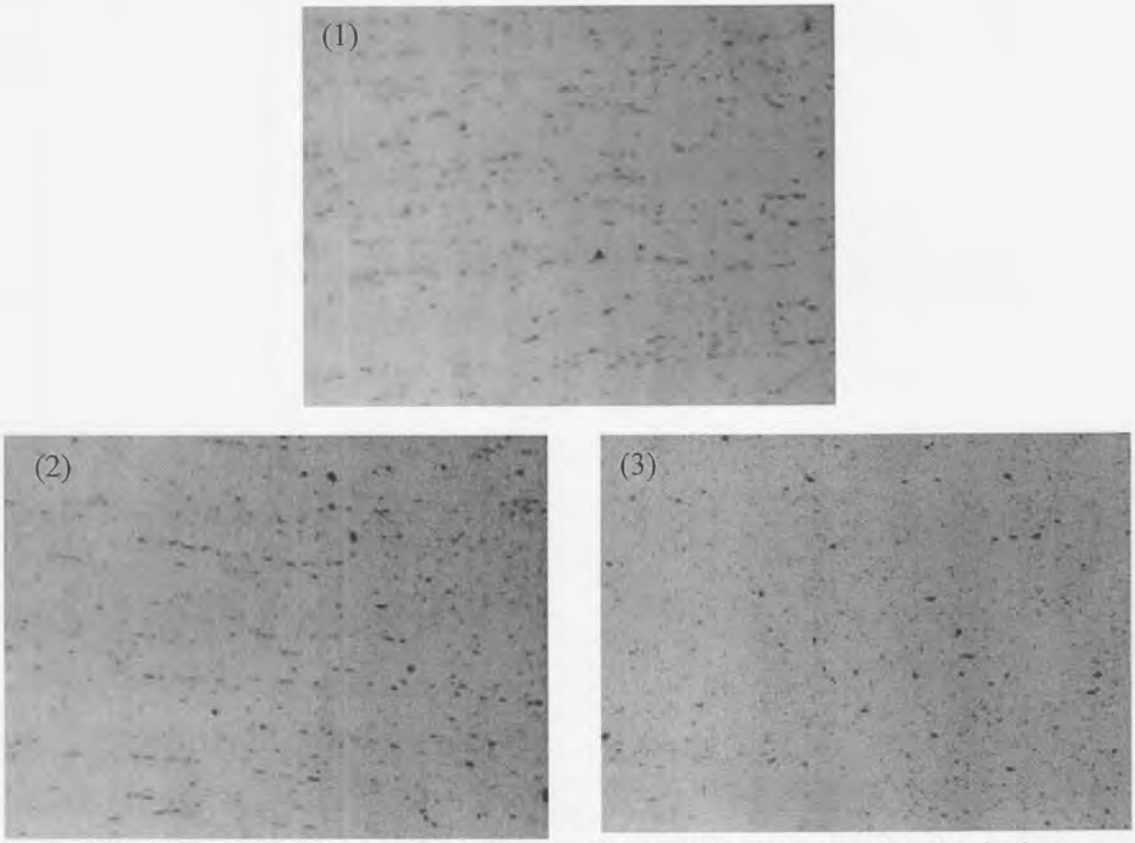

Figure 2-2: Light microscope images showing the carbide structures for the the base (1), the 2 % molybdenum (2) and the 2 % vanadium (3) alloys (100×)

2.1.3 Scanning electron microscopy

Scanning electron microscopy (SEM) was performed on pieces of sheet cut out of different places in the sheets (near the ends, in the middle, etc.). Electron dispersive spectroscopy (EDS) analyses performed on the 4 Mo and 4 V alloys confirmed the analytical analyses on the alloy contents of these materials. It also showed that the molybdenum and vanadium were evenly distributed throughout the sheets.

Some of the inclusions were analysed using EDS analysis. Because the inclusions are so small one cannot analyse only the inclusion and it is expected that part of the surrounding matrix was also included in the analysis. This gives an apparent alloy content somewhere between the matrix and the inclusion and therefore gives only an indication of which elements are enriched in the inclusion. It was found that the inclusions in the 4 Mo alloy had a high chromium to molybdenum ratio. This confirms the fact that one would expect predominantly chrome carbides in this material with most of the molybdenum in solid solution. The inclusions in the vanadium alloy on the other hand showed a very high vanadium to chromium ratio which in turn confirms that vanadium is a stronger carbide former than chromium and that one would expect most of the carbon and nitrogen to be taken up by vanadium. Figure 2-2 also supports this with the base (Figure 2-$2_{(1)}$) and the 2 Mo (Figure 2-$2_{(2)}$) alloys showing inclusion stringers compared to the 2 V alloy (Figure 2-$2_{(3)}$), which shows an evenly dispersed inclusion structure. The layered structure was formed because the chromium carbides form predominantly on grain boundaries, which are

flattened by the rolling of the plate. The inclusions in the vanadium alloys on the other hand form throughout the matrix and not preferentially on the grain boundaries.

2.2 Potentiodynamic scanning

2.2.1 Sample preparation

Samples were cut from the 1mm thick annealed sheet of the seven different alloy compositions. Four samples were taken from each alloy. The samples were wet surface ground to a 120-grit finish.

2.2.2 Instrumentation and setup

These tests were performed at Mintek using their equipment and fixed setup for potentiodynamic and potentiostatic tests. The scans were performed in an 'Avesta' type pitting cell (~800 mℓ capacity) to prevent crevice corrosion [49]. The cell works on the basic principle that concentration of ions in the crevice, where the sample fits to the cell, is prevented. This is achieved by seeping pure water through filter paper which fills the gap between the sample and the cell. A saturated calomel reference electrode, which was in electrical junction with the electrolyte through a luggin probe, was used in this work and all pitting potentials are quoted in reference to this. The working, counter and reference electrodes were connected to a potentiostat, which was in turn connected to a computer with software for controlling the potential and recording the current.

2.2.3 Test procedure

Potentiodynamic scanning tests were performed in a 3.56% sodium chloride solution that was not de-airiated before the tests. The test surfaces of the samples were exposed to the solution for periods ranging from 30 to 60 minutes while the potential was monitored continuously. Scanning was started after the potential had stabilised at the corrosion potential. Scanning was performed at a scan rate of 20 mV per minute at room temperature, starting at the corrosion potential and ending the test when the current reached a value of 2.5 mA. The exposed surface of each sample had an area of 5 cm^2. After the scanning tests the sample surfaces were inspected for the presence of crevices and pits under a stereo microscope. The samples were surface ground again and the test was repeated for each sample. Data for the samples showing crevices was discarded. Six valid polarisation curves were determined for each alloy. Figures 2-3 and 2-4 show typical polarisation curves generated with the potentiodynamic scanning of these samples. The passive and pitting regions are clear. The exact potential of transition from passive to stable pitting corrosion is not always clearly defined due to gradual current increases and electrochemical noise. To overcome this problem the pitting potential was defined, for this work, as the potential where the current density reaches 0.05 mA/cm^2. This critical current density size was chosen so that it is in the pitting region for al the polarisation curves attained, but also as close to the transition, from passive to stable pitting, as possible.

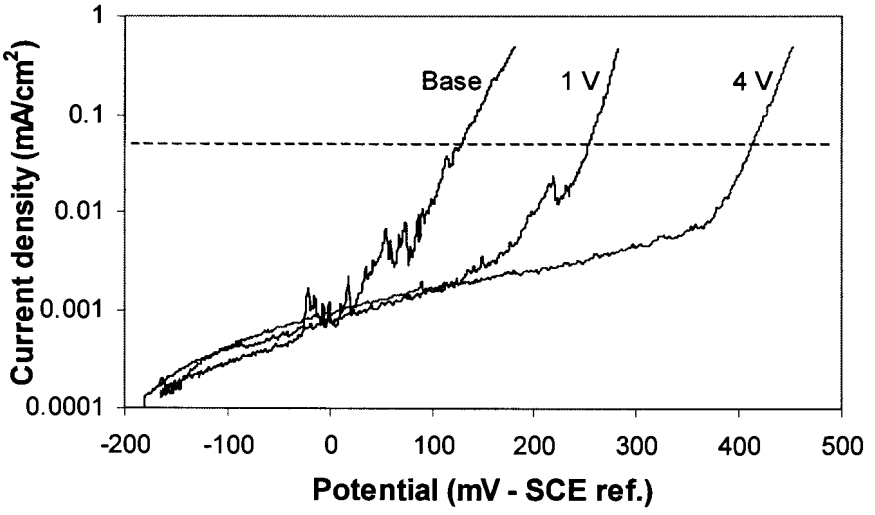

Figure 2-3: Experimental potentiodynamic scans on the 1 and 4% vanadium-containing alloys in relation to that of the base alloy (18Cr). The broken line indicates the current density used to define the pitting potential.

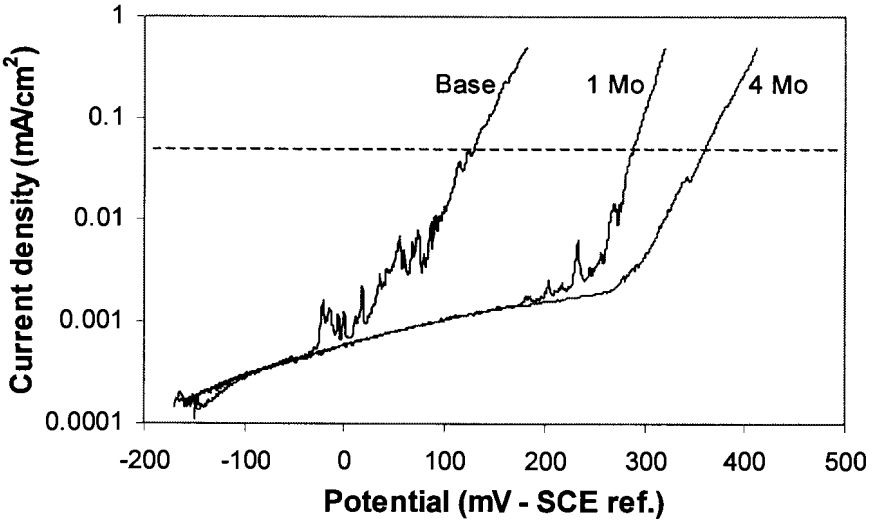

Figure 2-4: Experimental potentiodynamic scans on the 1 and 4-% molybdenum-containing alloys in relation to that of the base alloy (18Cr). The broken line indicates the current density used to define the pitting potential.

2.3 Artificial pit tests

To study the dissolution characteristics within growing pits it was necessary to isolate a single growing pit. The idea with this test work was to create a single pit artificially and to measure the growth kinetics of this pit.

2.3.1 Electrodes

'Lead-in-pencil' electrodes were used for this test (See Figure 2-7). These electrodes consist of a metal wire set in resin. The wire was dissolved from one end to form a pit in the resin.

The wire was manufactured by cold rolling 1-mm plate down to 0.5 mm. The plate was heat treated at 950°C and water-quenched to achieve the same microstructure as found in the 1mm plate. The plate was cut into 0.5 mm × 0.5 mm, square wire electrodes using a diamond cutting wheel. Electrical wire was soldered to one end of the electrodes before they were set into resin.

The pits were grown in a 1M NaCl solution with the potential held at 1V relative to the reference electrode; the charge was monitored. The pits were grown to a depth of 0.5 mm by controlling the amount of charge. The required amount of charge was determined to be 3.71 C by assuming that the alloys consist only of 18% Cr and 82% Fe with Fe going to Fe^{2+} and Cr going to Cr^{3+}. The calculations are shown in Appendix C.

This value is only an estimate and each pit was grown to almost this value and then its depth was measured using an optical microscope. The charge necessary to grow the pit up to the full depth was then re-calculated and the pit growth completed. The growth process was under diffusion control and the current density vs time behaviour is shown in Figure 2-5. Figure 2-6 shows an optical image of a typical artificial pit.

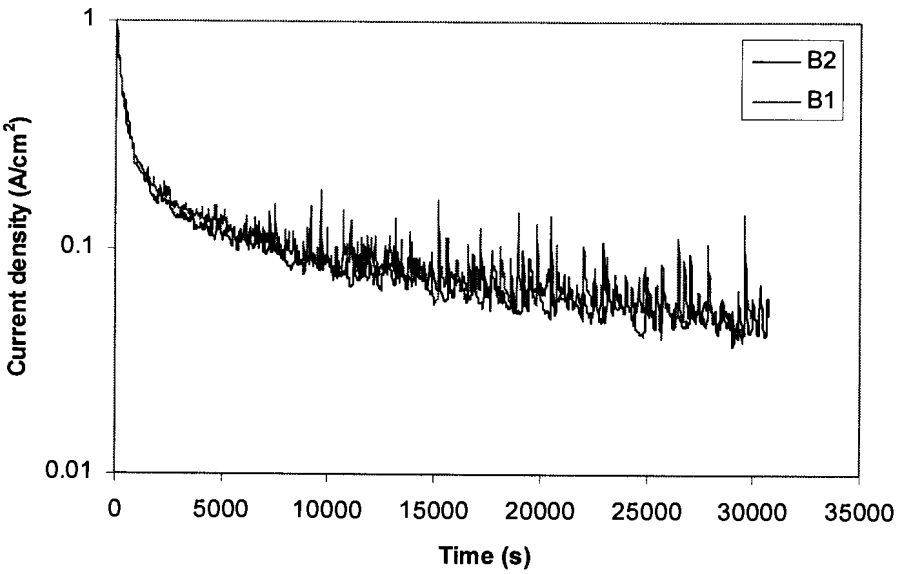

Figure 2-5: Current density – time relationship showing the diffusion controlled growth of artificial pits in the base alloy

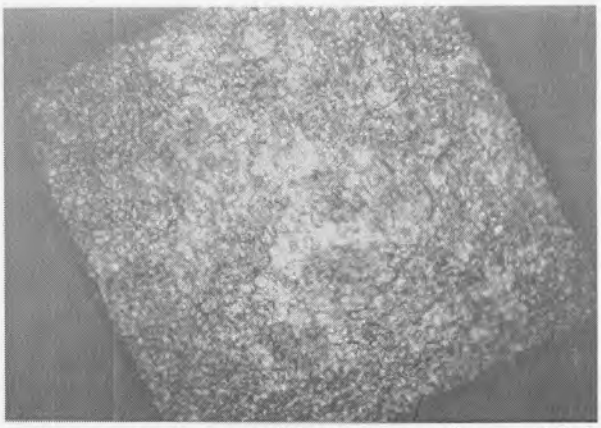

Figure 2-6: Light microscope image of the bottom of an artificial pit (2 Mo alloy) showing the metal surface (after test has been run) and the resin sides (which are out of focus)

2.3.2 Instrumentation and Setup

Figure 6 gives a schematic presentation of the electrochemical cell. A Ag/AgCl reference electrode was used and all potentials are given in relation to this. The reference electrode was brought in to electrical contact with the test solution through a luggin probe filled with saturated KCl solution. A carbon counter electrode was used in the tests. Figure 6 also shows the 'lead-in-pencil' work electrode in place. The potential was controlled by a Solartron instruments SI1287 Electrochemical Interface potentiostat. Impedance measurements were made possible through a Schlumberger SI1260 Impedance/Gain-Phase analyser. A personal computer was used to record the potential and current during the tests.

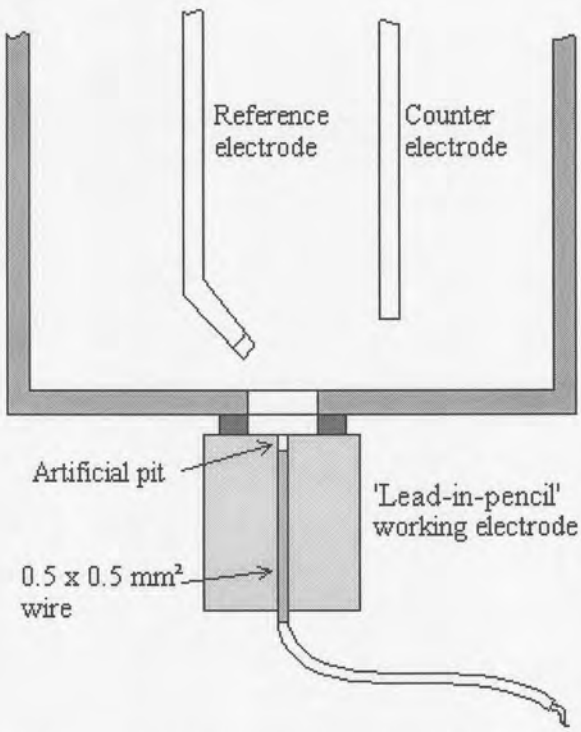

Figure 2-7: Cell for artificial pit tests (showing 'lead-in-pencil' electrode)

2.3.3 Determining activation controlled dissolution kinetics

The last bit of the pit depth (~50 μm) was grown in the same solution in which the polarisation test was subsequently carried out in, without intervening removal of the electrode from the solution (1M NaCl) (to prevent a passive layer from forming by exposure to the atmosphere). After growth to the final depth, the pits were rinsed (while in the cell) with the test solution by using a syringe with a needle to remove corrosion products before the polarisation test was run.

The tests were performed at room temperature (~25°C). A Ag/AgCl reference electrode was used and all potentials are quoted in reference to this (+0.2 V vs SHE).

Figure 2-8 shows the potential control schedule for the test. It was divided into three different stages as indicated. Firstly the enriched solution inside the pit was stabilised at a relatively high potential. In this stage a salt film forms inside the pit. There is a steep increase in the current as an enriched solution forms fairly quickly inside the pit followed by a slow decrease in the current as the reaction stabilises in a diffusion-controlled state. In the second stage the potential was then dropped to a potential where the salt film dissolves. This was marked by sudden decrease in the current with a subsequent small increase in current that reached a maximum after a certain time which dependend on the alloy. When the current reached a maximum the potential was scanned back in a positive direction until the current reached the same value as in first stage. It can be seen that the potential was considerably lower than it was in the first stage. Small potential ramps (20mV) were applied to confirm that the reaction was activation controlled. An impedance measurement was also run at this stage to determine the solution resistance. The potential was then pulsed down for short intervals to determine the polarisation curve for the alloy.

For the base alloy it was found that diffusion control inside the pit (stage 1) was stabilised at a potential of 200 mV and film dissolution (stage 2) was achieved by lowering the potential to -400 mV for 30 to 60 seconds. For the vanadium alloys this schedule also worked. However, for the molybdenum containing alloys it was found that the potential for the stabilisation of a salt film inside the pit was dependent on the molybdenum content, with a higher potential needed for a higher molybdenum content. For the 1% molybdenum content 200 mV could be used, but for the 2 and 4% additions, 300 and 400 mV respectively, were necessary to stabilise diffusion controlled dissolution. The potential for salt film dissolution also had to be moved to higher potentials to prevent the enriched pit solution from being lost.

A repeat run (of the artificial-pit polarisation measurements) was completed for each alloy yielding the same results.

2.3.4 Determining the diffusion controlled dissolution kinetics

Electrodes were ground flat (800 grit). A 1M NaCl solution was used and the tests were performed at room temperature (23±2)°C. The same setup was used as for the above mentioned tests. The potential was controlled at 1 V anodic to the corrosion potential to ensure the dissolution took place well inside the diffusion-controlled region. Experiments were run for 8 to 10 hours to reach a depth of 1 mm inside the pit. Figure 2-5 shows a typical current density - time relationship.

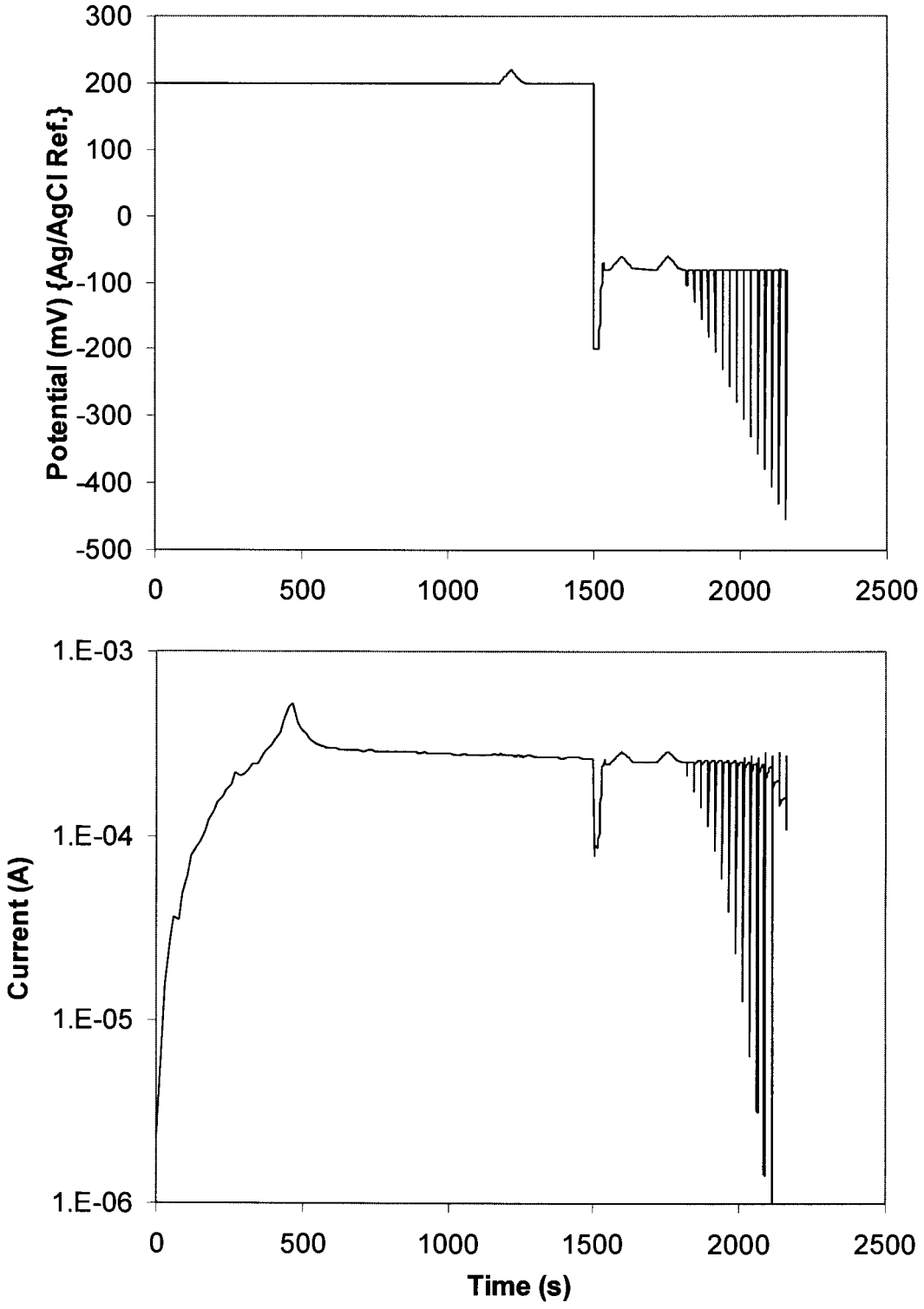

Figure 2-8: Potentiodynamic control and corresponding current measurement during artificial pit electrochemical test

2.4 Pit initiation tests

In order to measure the small current events the setup and instrumentation had to be very sensitive to small current changes and isolated from external signals. It was also necessary to use working electrodes with relatively small exposed surfaces to limit the number of events taking place during the experiment, to be able to identify individual events, but with large enough surfaces to obtain sufficient measurements to achieve statistical significance.

2.4.1 Electrodes

Small electrode wires were manufactured from the 1 mm plate in the same way as for the artificial pit electrodes. These 0.5 mm × 0.5 mm wires were electrically connected and set in tubes to expose only about 20 mm of the wire. The sides and tip of the wire were wet ground with 800 grit grinding paper. A stable passive layer was then formed on the surface by placing the electrodes in 15 % nitric acid at 55°C for 20 minutes. The test described in paragraph 2.4.3 was performed on a electrode in the fully passive state to confirm that the passive layer did in fact prevent any pits from forming. A 2 mm length of the wire 2 mm away from the end was then wet ground to 1200 grit to remove the passive layer. The electrodes were washed in acetone in an ultra-sonic bath immediately afterwards to remove any contaminants from the surface. They were then rinsed in distilled water and immediately placed in the test solution. The potential of the electrodes was held at -100 mV (Ag/AgCl ref.) for 10 minutes to stabilise the electrode surface at this potential before the test commenced.

2.4.2 Instrumentation and setup

An aluminium case was used as a Faraday cage, which was needed to isolate the cell and electrodes from external signals. Also in the Faraday cage was a battery potentiostat. This allowed for the cell to be completely isolated from signals in the electric power supply. A battery sweep generator was used to scan the potential at the desired rate and from the desired setpoint. The potential was measured using a Keithley 614 electrometer. A Keithley 428 current amplifier was included in the circuit to measure the current. The current amplifier allowed for the gain to be adjusted during the experiment in order to get maximum sensitivity on the current measurements. It also had a filter option to filter out background noise. A Yokogawa AR 1100 analysing recorder recorded both the potential and current against time on different channels. The test was controlled from and recorded data captured on a computer.

2.4.3 Potentiodynamic scanning and data logging

The potentiodynamic scanning was performed at 25°C (±1°C) in a 3.56% NaCl solution. A scan rate of 2 mV per second was used and the scanning stared at a potential of –100 mV (Ag/AgCl ref.). The current and potential readings were logged at a rate of 50Hz. The filter was activated and set to a 30 ms rise time and the tests were started with the gain setting (output voltage divided by current) on the current amplifier set on 10^6 Ω. At these settings the noise level was around 1 nA.

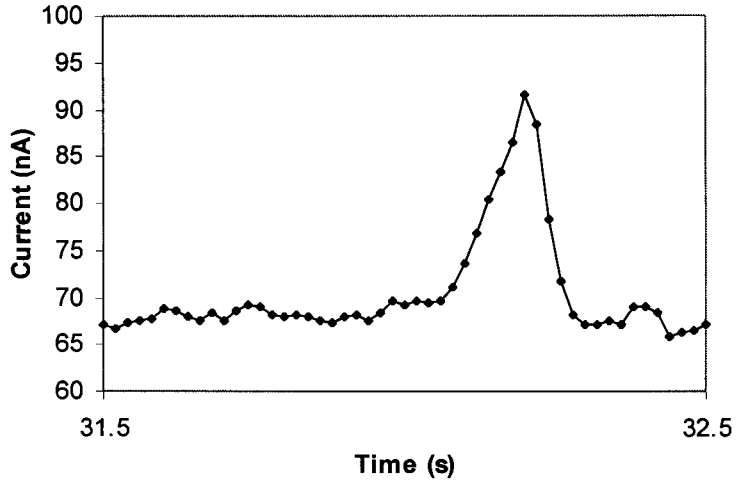

Figure 2-9: Current – time curve showing the frequency of recording of data points over some electrochemical events

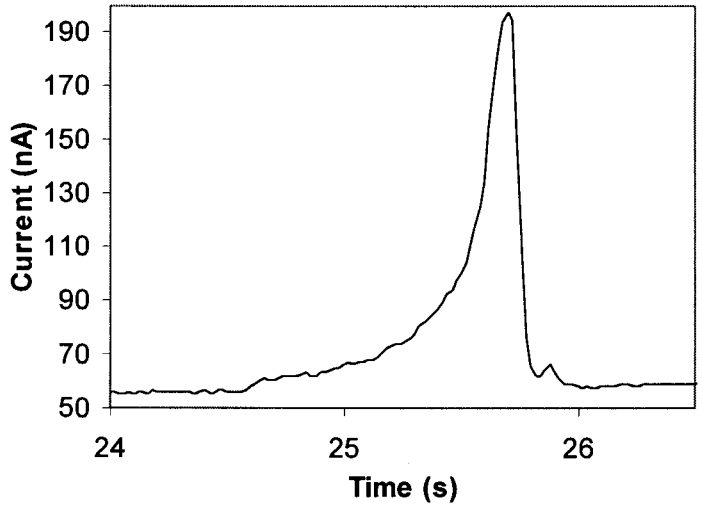

Figure 2-10: Two typical current events

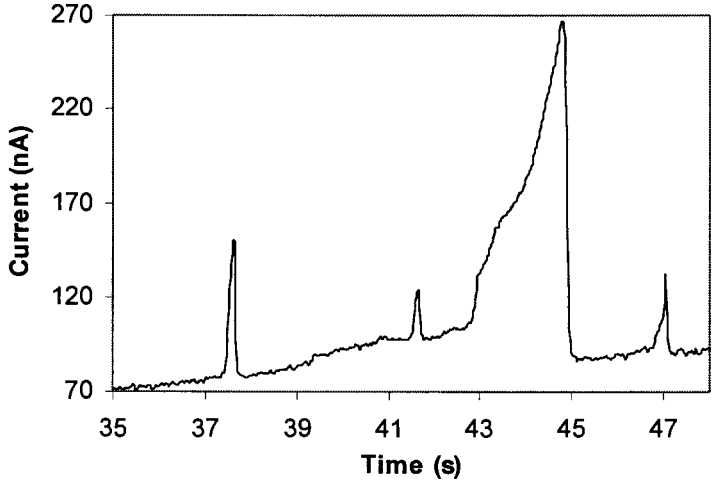

Figure 2-11: Current – time curve showing one 'big' and three smaller electrochemical events

2.4.4 Determining the metastable pit frequency

The metastable pits were counted manually. Pits were counted if they could visibly be distinguished from the background noise. Figure 2-9, Figure 2-10 and Figure 2-11 show the typical shape of the current–time curve of some electrochemical events. Because the electrochemical events overlapped, individual events were identified by the sudden drop in current which marks the end of metastable growth.

2.4.5 Determining the maximum current density inside the metastable pits

The amount of charge that flowed for a pit was determined by integrating the current over the time (life of the pit) curve and subtracting the background charge. From this the size of the pit could be determined by making the same assumptions about the dissolution reactions taking place as in paragraph 3.1 as well as the assumption that the pits are hemispherical. Pistorius and Burstein experimentally showed this assumption to be reasonable [20]. The inside surface area of the pit is then easily determinable. The maximum current density is determined as the difference between the peak current density for the electrochemical event and the background current for the same time.

2.4.6 Quantitative and qualitative visual inspection of metastable pits

The surfaces of the small electrodes were examined using a JEOL 840 scanning electron microscope. One of the four side sides of each of two electrodes per alloy was examined. 112μm × 85μm areas were picked at random and then all the pits present inside the area were inspected. In this way the apparent size distribution for the pits could be determined. Three types of pits were distinguished: open pits, closed pits (pits covered with a perforated cap) and those pits where it is not possible to determine with certainty if they are open or closed.

3. Results and discussion

3.1 Effect of vanadium vs molybdenum

Figure 2-3 and 2-4 show typical polarisation curves as determined for the experimental alloys. See Appendix B for different scans of each alloy plotted on the same graph. One of the first observations made when looking at the polarisation curves for the different alloys is the positive shift in pitting potential brought about by an increase in the molybdenum and vanadium contents. The base metal produced an average pitting potential of ~130 mV relative to saturated calomel electrode reference. An addition of 1% of molybdenum or vanadium brought about a relatively large increase in the transition potential of about 130 mV. Further increases in the molybdenum and vanadium contents increased the pitting potential further but the increments were smaller.

It is believed that alloying elements locked in carbides and nitrides do not contribute to the resistance to corrosion. In an attempt to isolate the effects which vanadium and molybdenum have on the pitting potential it was decided to compensate for the 'loss' of these elements to these precipitates. Vanadium is known to be a strong carbide and nitride former. As mentioned earlier, scanning electron microscopy energy dispersive spectroscopy (SEM-EDS) analyses of the precipitates in the vanadium containing-alloys showed very high vanadium to chromium ratios. This confirmed that the precipitates consist primarily of vanadium carbides (VC) nitrides (VN) or carbo-nitrides (V(CN)). Molybdenum is not as strong a carbide or nitride former and the SEM-EDS analyses of the precipitates showed low molybdenum to chromium ratios. It was therefore assumed that all the molybdenum is in solid solution in the molybdenum-containing alloys while chromium takes up all the carbon and nitrogen. The chromium content is high and the percentage chromium lost to precipitates is small and it is believed that this does not result in large changes in the pitting potential. For the vanadium-containing alloys the percentage vanadium lost to precipitates is considerable and a noticeable effect on the pitting potentials is expected. If the stoichiometric ratio of vanadium to carbon or nitrogen is approximated as 1:1 the vanadium still in solid solution is estimated as shown in Table 3-1. In Figure 3-1 the pitting potentials are plotted against these calculated effective vanadium and molybdenum contents.

Table 3-1: Weight percentages of vanadium and molybdenum estimated to be available for influencing the pitting potential

Alloys	*Mo*	*V*
Base	0.03	<0.01
1 V	0.03	0.72
2 V	0.03	1.69
4 V	0.03	3.56
1 Mo	0.92	0.01
2 Mo	1.93	0.01
4 Mo	3.80	0.01

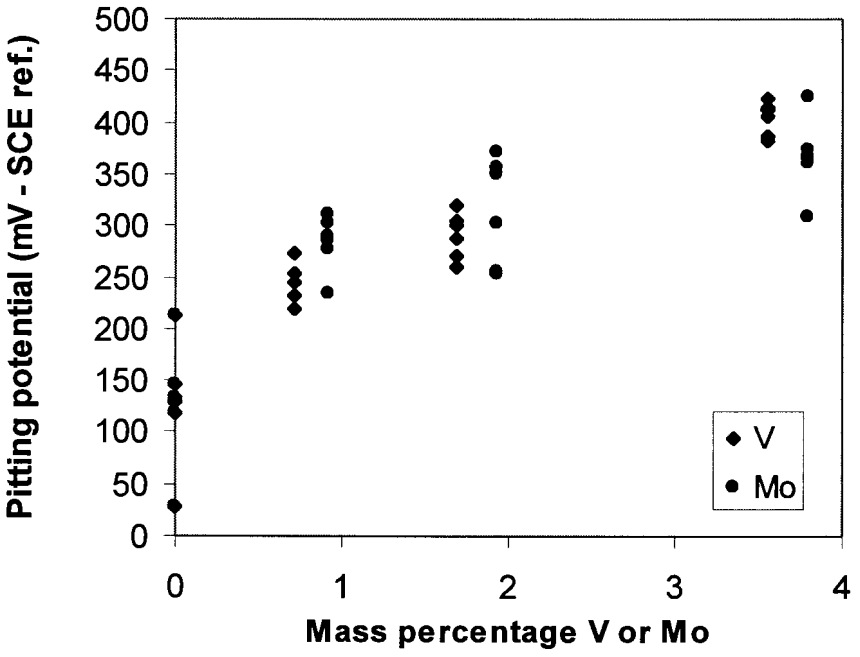

Figure 3-1: Pitting potential vs. alloy content for experimental alloys

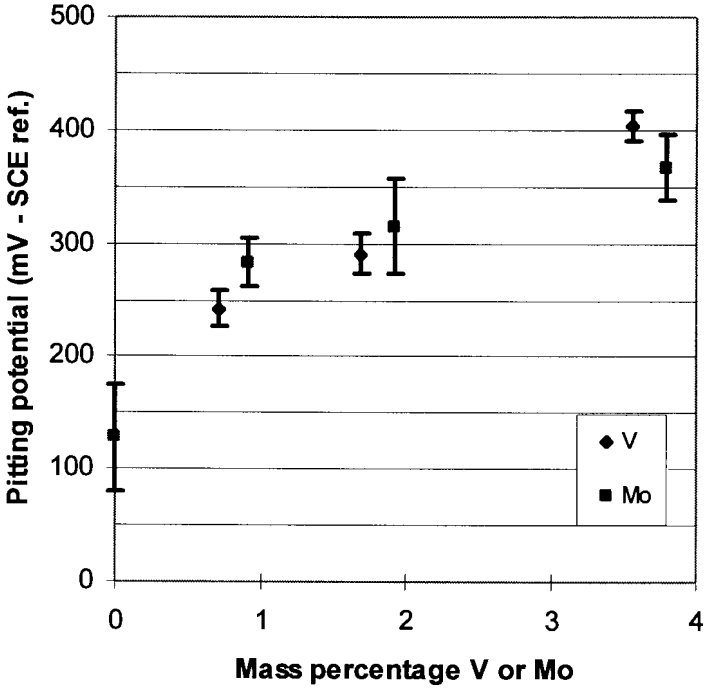

Figure 3-2: Pitting potentials vs. alloy content. The error bars show 95% confidence intervals on the average pitting potential.

Figure 3-2 shows the average pitting potential and the 95% confidence intervals plotted against the calculated vanadium and molybdenum quantities in solid solution. An increase in molybdenum shows the expected increase in pitting potential. Vanadium additions gave an increase in pitting potential of the same extent as molybdenum on a weight percent basis. The similarity in the 1 and 2% region confirms previous work [47]. At the 4% level vanadium seems to give slightly superior

resistance with less scatter in the pitting potential. One of the aims of this project was to determine a pitting resistance equivalent for vanadium in solid solution. As indicated in paragraph 1.2, the coefficient for Mo is generally accepted as 3.3. The determination of a pitting resistance equivalent rests on the general assumption that the relation between the pitting potential and the alloy addition is linear. On the basis of this assumption (which is in fact not supported by the current data) linear lines were fitted through the two sets of data in Figure 3-2 and a ratio between the gradients was determined. The coefficient for molybdenum was then multiplied by this ratio to determine the coefficient for vanadium, which yielded a value of 3.7 – confirming the similarity between vanadium and molybdenum (on a mass basis).

3.2 Mechanisms

The second aim was to compare the mechanisms at work for molybdenum and vanadium respectively and to try to explain why an improvement in the localised corrosion resistance is brought about by additions of vanadium.

3.2.1 Electrochemical noise

There is a more subtle difference between the polarisation curves for the vanadium and the molybdenum. The vanadium alloys, like the base metal, show more electrochemical noise in the passive region compared to the molybdenum containing alloys (see Figures 2-3 and 2-4). This electrochemical noise is believed to be related to the formation of metastable pits. The differences between the polarisation curves of the vanadium and molybdenum–containing alloys possibly indicate a difference in the mechanisms, which are at work for these two groups of alloys.

3.2.2 Active dissolution controlled kinetics

The assumed mechanism for molybdenum has been shown by many investigations to rely on the ability of molybdenum in solid solution to decrease the active current density on the dissolving pit surface by enriching on the metal surface itself [29,30,31,32,34,35]. This effect was best illustrated by tests where a single artificial pit is controlled in the active dissolution region while the polarisation data is being measured [32,34]. Similar tests were performed on the current experimental alloys to directly compare the effect of vanadium on the active dissolution rate with that of molybdenum.

Figure 3-3 shows the polarisation data for the different experimental alloys as determined by the test procedure described in paragraph 2.3 above. The slopes of the curves are similar to those determined in previous artificial pit work [32]. The effect of the molybdenum is clearly visible as the polarisation curve is shifted to lower current densities with each increase in molybdenum content. A 2% molybdenum addition to the 18Cr ferritic stainless steel caused a shift of the Tafel line of about 100 mV compared to the 60 mV shift Newman found with a 2.7% molybdenum addition to a 17Cr-11Ni austenitic stainless steel. At the 4% addition level a current density reduction of around 2 orders of magnitude was measured. This corresponds well with other work on 18% Cr ferritic stainless steels where the anodic behaviour for samples were measured in 1N HCl and a similar drop in current density was brought about by

4.75% molybdenum addition to the alloy [27]. The vanadium containing alloys however showed no discernible shift of the Tafel lines and all show polarisation behaviour similar to that of the base metal. It can therefore be concluded that vanadium has no effect on the active dissolution reaction rate inside the artificial pits. There is thus definitely a difference in the mechanisms for the effect of vanadium and molybdenum on pitting resistance.

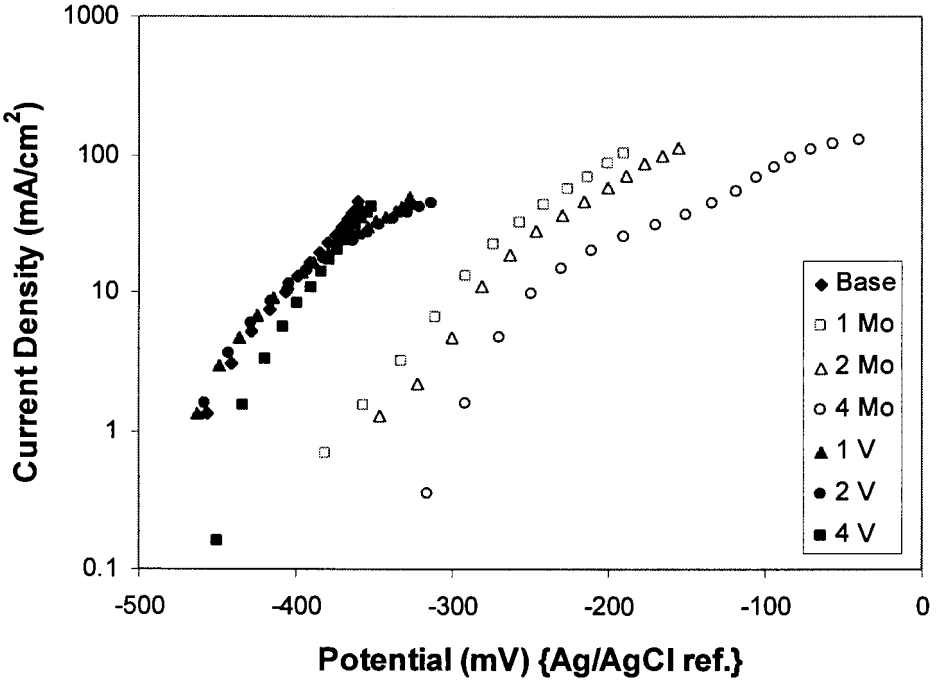

Figure 3-3: Polarisation data for artificial pits – IR corrected

3.2.3 The frequency of formation of metastable pits

The dependence of pitting resistance on the rate of formation of metastable pits was expressed by Williams *et al.* [50] as:

$$\Lambda = \lambda \exp(-\mu\tau_c) \quad \text{.....(3-1)}$$

where Λ is the rate of formation of stable pits, λ the rate of formation of metastable pits, μ the probability of a metastable pit repassivating and τ_c the critical time beyond which pits are considered stable if they are still active. It can therefore be expected that a change in λ will lead to a change in Λ. If vanadium were to cause a decrease in the frequency of metastable pit formation compared to the base metal and the molybdenum alloys, an increase in pitting resistance is possible.

Figure 3-4 shows the measured pit formation frequency as a function of the potential as determined performing potentiodynamic sweeps at 2mV/s. The frequencies were determined by counting the number of metastable growth events in each 50 mV interval (25s interval). There is a clear increase in the frequency of these events with potential. This does not agree with work done by other investigators [20,26].

It can further be seen that an increase in vanadium content lowered the frequency of distinguishable metastable pits for a given potential. An increase in molybdenum

however caused an even bigger decrease in the metastable pitting frequency over most of the potential range of interest for each addition level. There is therefore no improvement of the vanadium containing alloys over the molybdenum alloys in reducing the frequency of pit formation and the mechanism for vanadium is therefore believed not to be primarily associated with the frequency of pit formation.

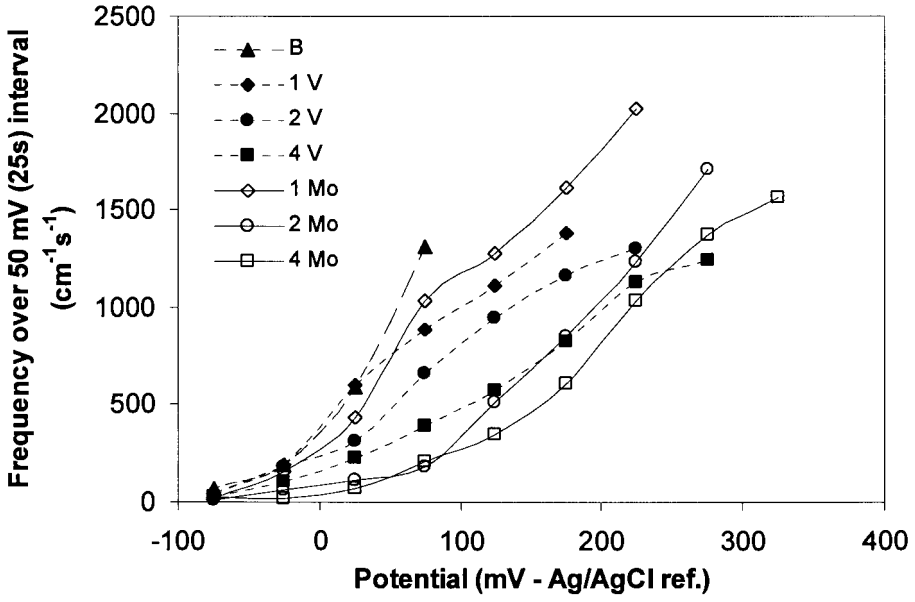

Figure 3-4:Metastable pit initiation frequency vs potential for different alloys

3.2.4 Dissolution rates within metastable pits

The current densities inside the metastable pits were determined according to the procedure described in paragraph 2.4.5. In Figure 3-5 the peak current densities of the metastable pits are plotted against potential. The current densities do not seem to be a function of the potential over the potential range measured. This is also not in agreement with the work by Pistorius and Burstein who measured the current densities for metastable pits in type 304 stainless steel [20]. They showed that the average current densities for metastable pits initiated at higher potentials was higher although the current densities of a pit already initiated does not change with a change in potential. This was believed to be related to the more open geometry pit initiation sites, which became accessible at higher potentials.

The molybdenum however caused a definite reduction in the current density inside the metastable pits. The average peak current densities for the metastable pits are 3.46±0.23 A/cm^2 (95% confidence interval) for the base metal, 2.75±0.15 A/cm^2 for the 4% vanadium alloy and 1.27±0.10 A/cm^2 for the 4% molybdenum alloy. Comparing these values to the curves in Figure 3-3, it can be seen that the metastable pits grow at current densities higher than the polarisation data that could be determined for the artificial pits. The molybdenum also only caused a drop of a little more than 50% in the dissolution rate as determined for the metastable pits compared the shift of about 2 orders in the current density for the artificial pit. This also indicates that the shift in current density seen here is not a direct effect of

molybdenum lowering the active current density. No simple direct effect is expected, since the pits presumably grow under diffusion control.

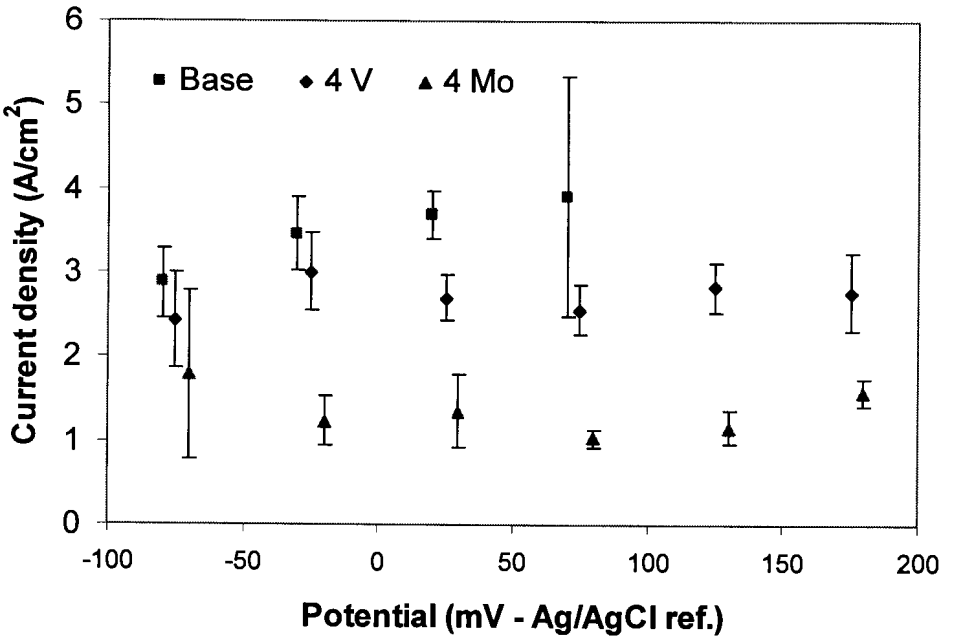

Figure 3-5: Current densities for metastable pits as a function of the potential. The error bars show 95% confidence intervals on the average values. The values for the base and the 4 Mo alloys have been shifted 5mV to clearly show the different confidence intervals.

Figures 3-7 a – c show the individual values of current density of the metastable pits as a function of the potential. The data points are scattered over the graph and there does not seem to be any pattern like an increase in the maximum current density, as we would have expected. There are a few features worth noting: The current density distributions around the mean current density seem to be slightly skewed with a few pits having higher current densities than what would have been expected by assuming normal distribution. The maximum current densities show the same decrease with molybdenum as the average values.

The average calculated pit radii over 50mV intervals, were plotted against the potential (shown in Figure 3-6). Apart from a slight increase in the radius with potential for the molybdenum alloy, no meaningful effects could be isolated.

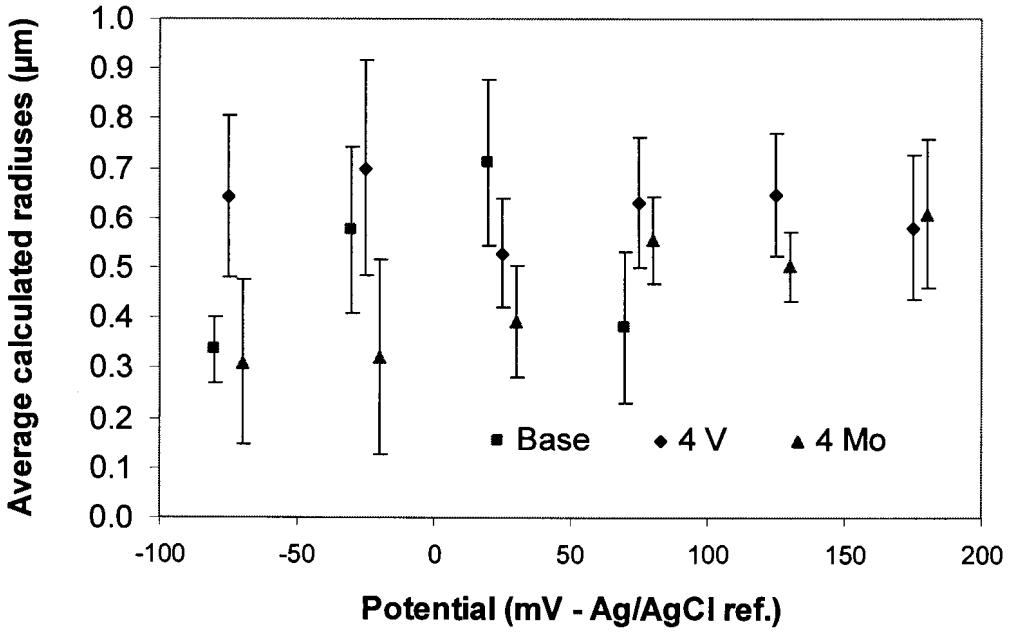

Figure 3-6: Average calculated radii for metastable pits (assuming hemisperical pits) as a function of the potential. The error bars show 95% confidence intervals on the average values. The values for the base and the 4 Mo alloys have been shifted 5mV to clearly show the different confidence intervals.

Figures 3-8 a – c show the maximum pit radius (calculated from the charge, assuming hemispherical pits) achieved by the pits as a function of the potential. These values too show a skewed distribution with average radii below 1 µm and a few pits with relative large radii. For the base alloy and the vanadium alloy there seems to be no real dependence of the pit radius on the potential, while for the molybdenum alloy the maximum pit radii seem to increase with an increase in potential.

Figures 3-9 a - c show the calculated stability products for the metastable pits (calculated at the maximum current, i.e. just before repassivation) as a function of the potential. These distributions are clearly skewed and the averages seem to stay fairly low with many of metastable pits initiating and repassivating at low stability products. From these graphs the increase of the maximum stability product with potential is clearly evident. This correlates well with the model proposed by Pistorius and Burstein [20]. The vanadium causes a decrease in the maximum recorded stability product of about 50% for a given potential relative to the base alloy while molybdenum lowers the maximum stability product by about one order of magnitude. This may explain the large shift in pitting potential brought about by molybdenum additions. The effect of vanadium additions on the pitting potential can apparently not be explained this way.

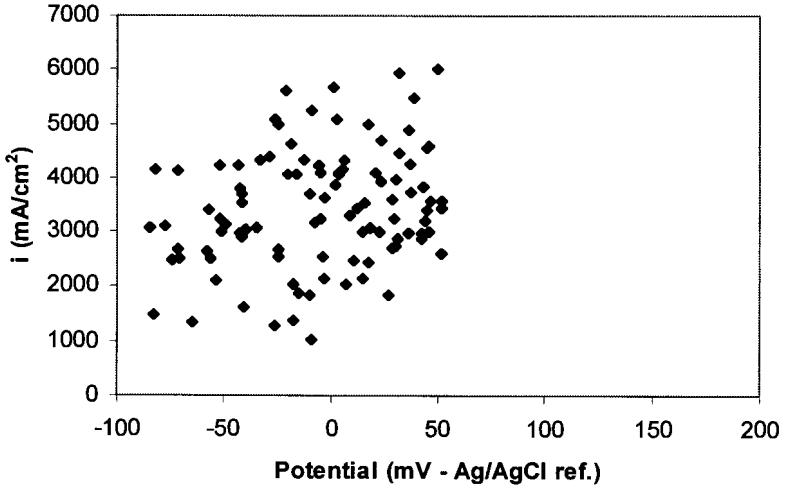

Figure 3-7a: Current density vs Potential for metastable pits in base alloy

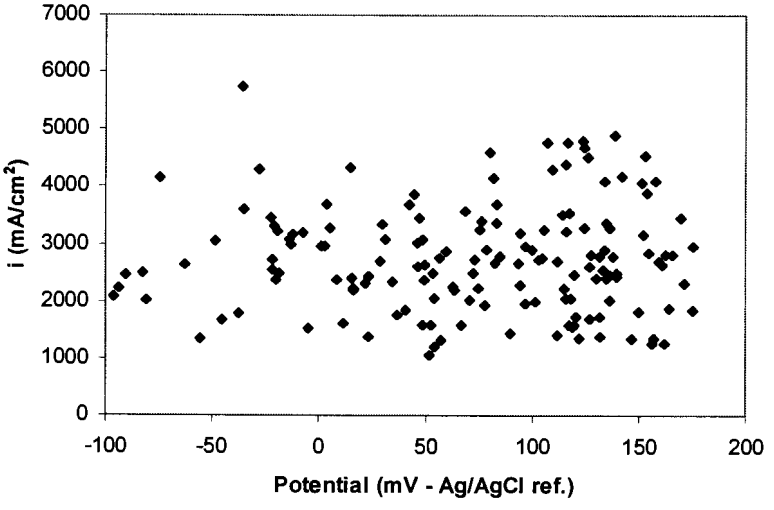

Figure 3-7b: Current density vs Potential for metastable pits in 4 V alloy

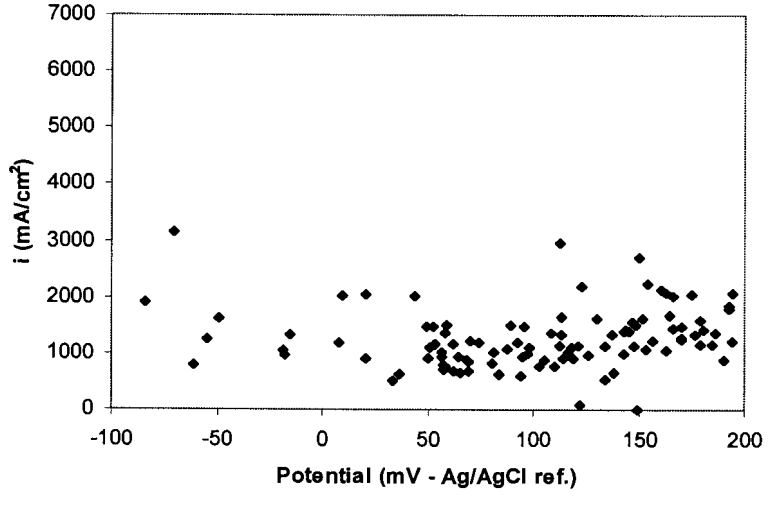

Figure 3-7c: Current density vs Potential for metastable pits in 4 Mo alloy

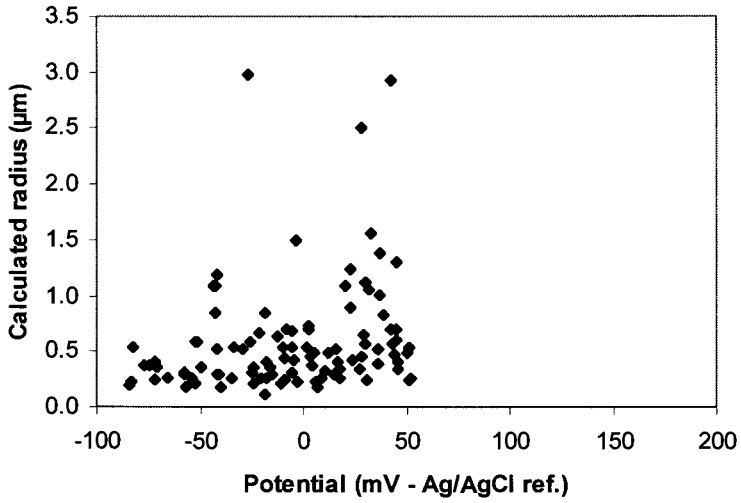

Figure 3-8a: Calculated pit radius vs Potential for metastable pits in base alloy

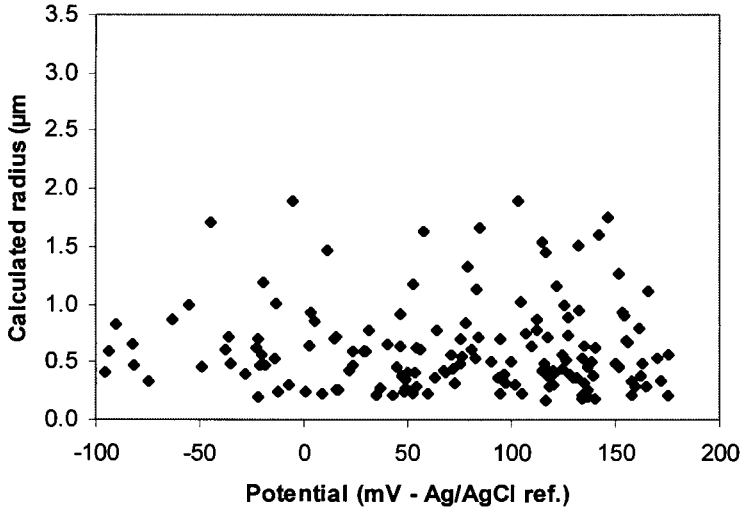

Figure 3-8b: Calculated pit radius vs Potential for metastable pits in 4 V alloy

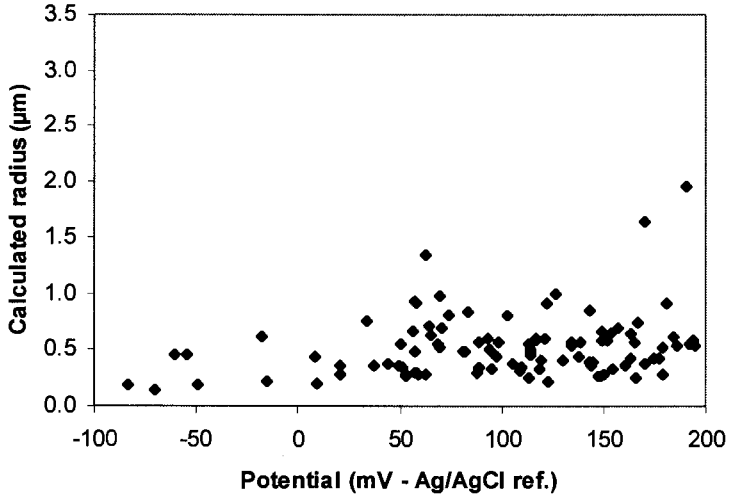

Figure 3-8c: Calculated pit radius vs Potential for metastable pits in 4 Mo alloy

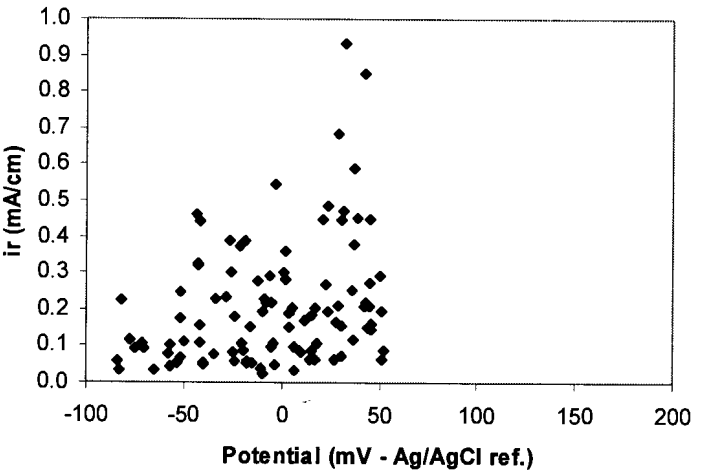

Figure 3-9a: Stability product vs Potential for metastable pits in base alloy

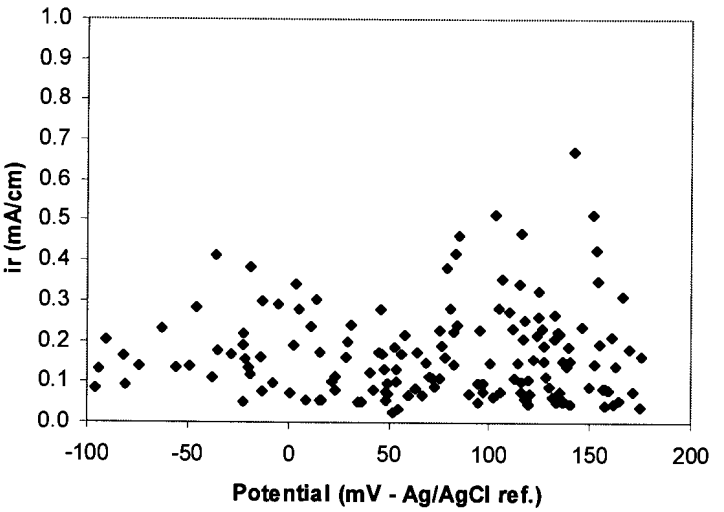

Figure 3-9b: Stability product vs Potential for metastable pits in 4 V alloy

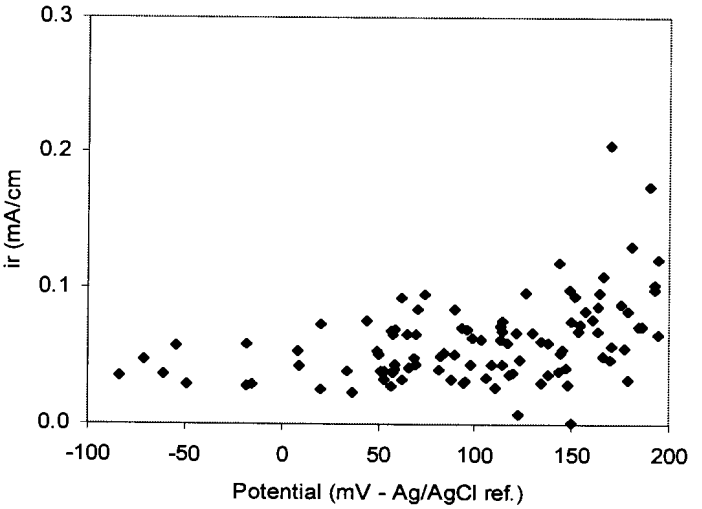

Figure 3-9c: Stability product vs Potential for metastable pits in 4 Mo alloy

3.2.5 Pit morphology

A microscopic inspection of the electrode surfaces used in the pit initiation tests was undertaken to try to find some clues as to the role of vanadium. Random areas were searched and the pit sizes as well as their cover morphology were recorded. The procedures are described in paragraph 2.4.6. Appendix E shows SEM images of typical micro pits.

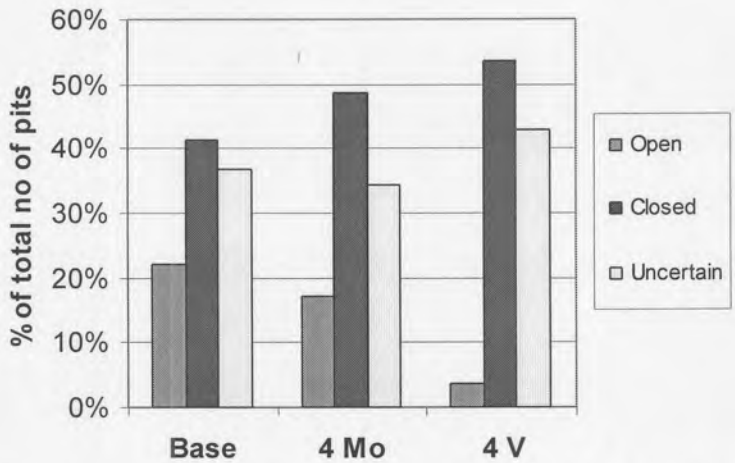

Figure 3-10: Comparison of cover morphology of metastable pits after pit initiation tests

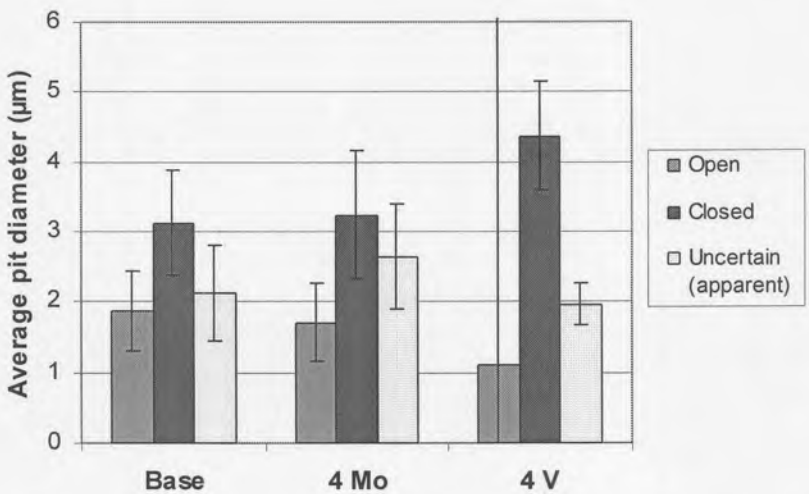

Figure 3-11: Comparison of apparent size of metastable pits after pit initiation tests

Figures 3-10 shows the ratios of open to covered pits for the base, 4 Mo and 4 V alloys. Figure 3-11 shows the average pit size for the different pit 'types' for the three alloys. These results did not really clarify anything about the mechanism of vanadium in increasing the pitting resistance of the 18Cr stainless steels. It is interesting to note however that the covered pits have higher average sizes for the all three alloys. This agrees with the mechanisms concerning the role of the pit cover [6,20,21] (see paragraph 1.5).

3.2.6 Diffusion controlled kinetics

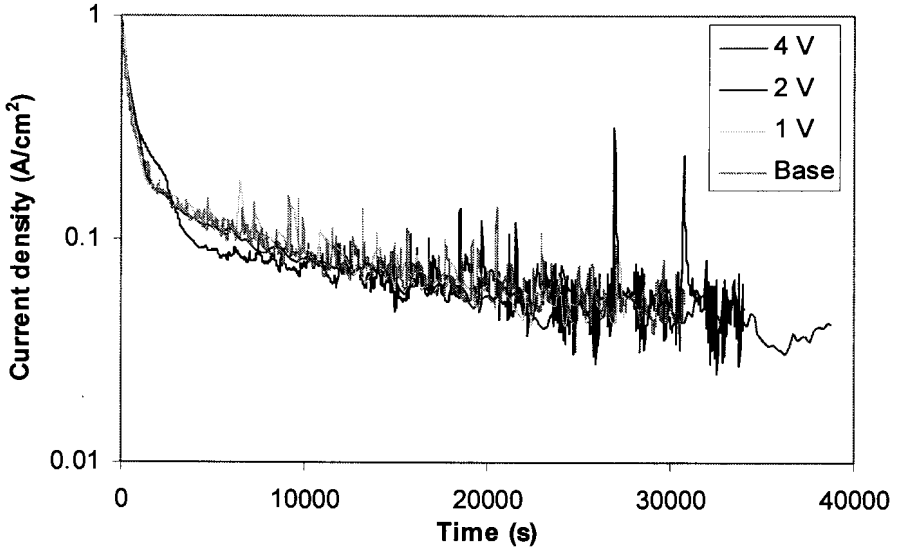

Figure 3-12: Current density vs time for the diffusion controlled growth of base and vanadium alloys

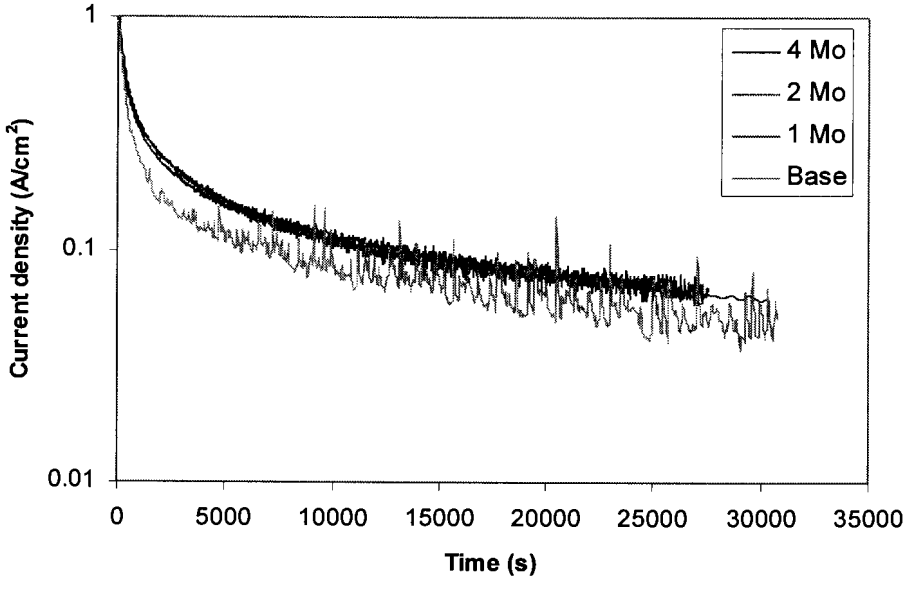

Figure 3-13: Current density vs time for the diffusion controlled growth of base and molybdenum alloys

The next aspect examined was the diffusion-controlled kinetics. Tests were performed as described in paragraph 2.3.4. Figure 3-12 and 3-13 plot the current decay curves for the vanadium and molybdenum containing alloys together with that of the base alloy. The vanadium alloys, like the base alloy, showed fairly noisy curves compared to the molybdenum containing alloys. For all the curves the current was approximately inversely proportional to the square root of the time as would be expected for diffusion control.

The molybdenum alloys seem to grow at higher current densities than the other alloys. By plotting the inverse of the square of the current density against time, linear relations were found and the molybdenum containing alloys were all shown to grow slightly faster. The vanadium alloys all showed basically the same growth rate as the base alloy and the role of the vanadium is therefore not to be found here (see Figures 3-14 and 3-15).

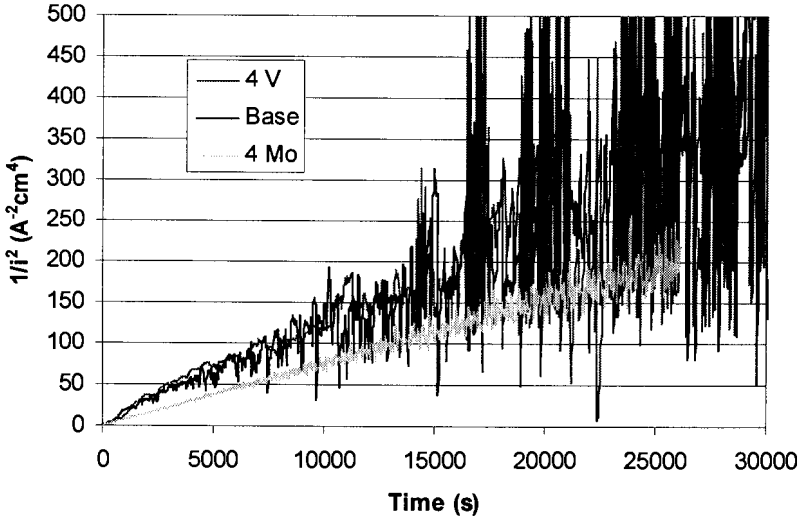

Figure 3-14: Inverse of the square root of the current density vs time

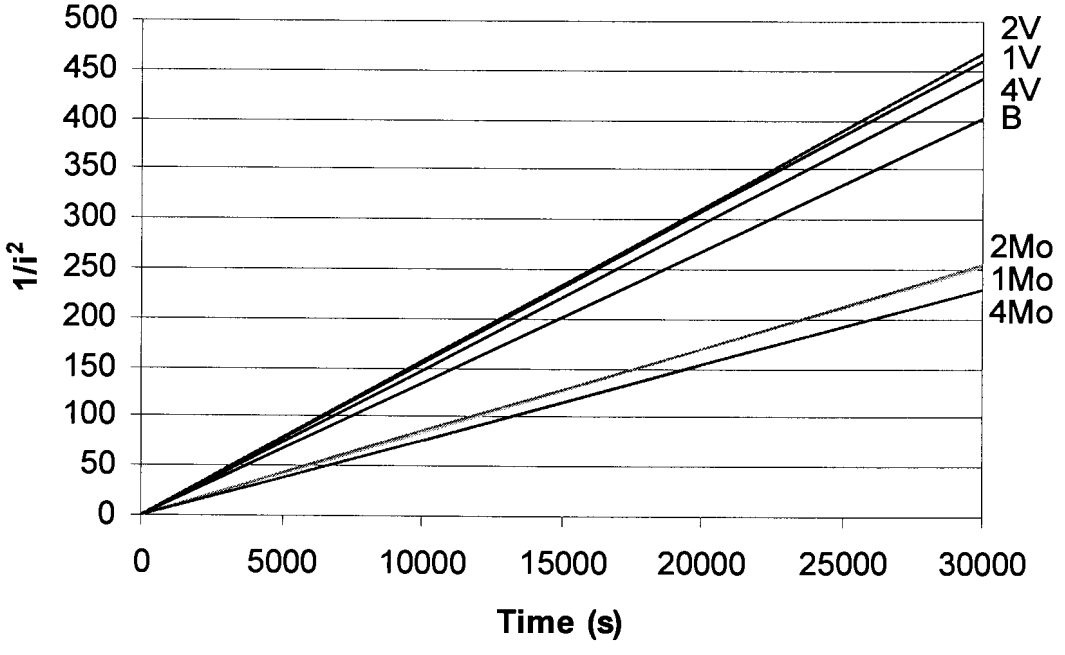

Figure 3-15: Inverse of the square root of the current density vs time. For clarity, only trend lines are shown to indicate the different dissolution rates.

3.2.7 Salt film properties

It was shown that as far as the formation of metastable pits is concerned there is no real difference between the molybdenum and the vanadium alloys (in the size range which could be measured). No real difference, which would help promote pitting resistance, was established by examining the pit morphologies of the vanadium and molybdenum alloys.

Looking at Figures 3-9 a-c it is clear that molybdenum limits the stability product which metastable pits are able to attain for a given potential. According to the model proposed by Laycock and Newman, molybdenum moves the transition potential (the potential where the transition from mixed activation/ohmic control to diffusion control takes place for metastable pits – thus the potential where the salt film forms) to a higher value [35]. It is believed that this transition is necessary if a metastable pit is to stand a change of reaching the required stability product and becoming stable.

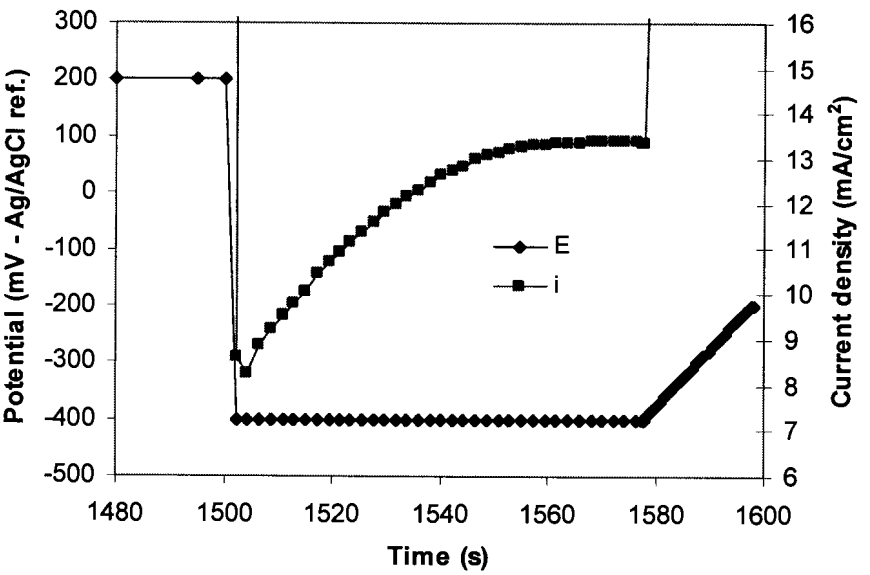

Figure 3-16:Dissolution of salt film in artificial pit experiment – base alloy

It is seen that the stability products attained for a given potential, for the vanadium alloy, is considerably larger than for the molybdenum alloy. If one can extrapolate this trend the vanadium alloy will have metastable pits reaching the critical stability product at potentials far lower than for the molybdenum alloy which would give a far inferior pitting potential. It is therefore believed that there must be some other factor, in the mechanism for the vanadium, which would prevent these metastable pits from reaching stability. This is perhaps related to the stability of the salt film. Figures 3-16 to 3-18 show the dissolving step during the artificial pit experiments. It is an enlargement of Stage 2 as indicated on Figure 2-7 and involves the dissolution of the salt film, which formed during growth of the pit at high potentials. The potential is dropped to dissolve the salt film to get the artificial pit in the active region in order to measure the active dissolution kinetics. It can be seen that the potential was kept low until the salt film has dissolved (as indicated by the current reaching a plateau) and

then scanned in an anodic direction before the enriched solution started disappearing (indicated by a reduction in current).

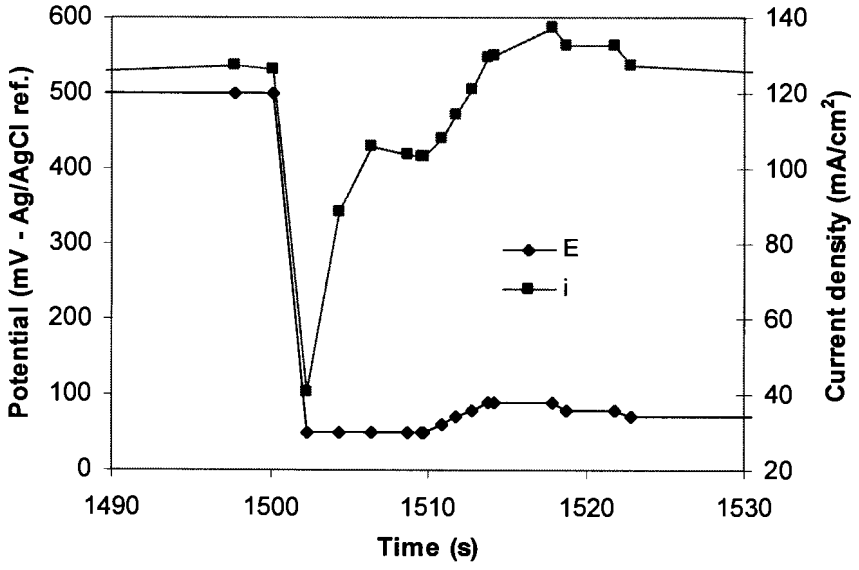

Figure 3-17:Dissolution of salt film in artificial pit experiment – 4 Mo alloy

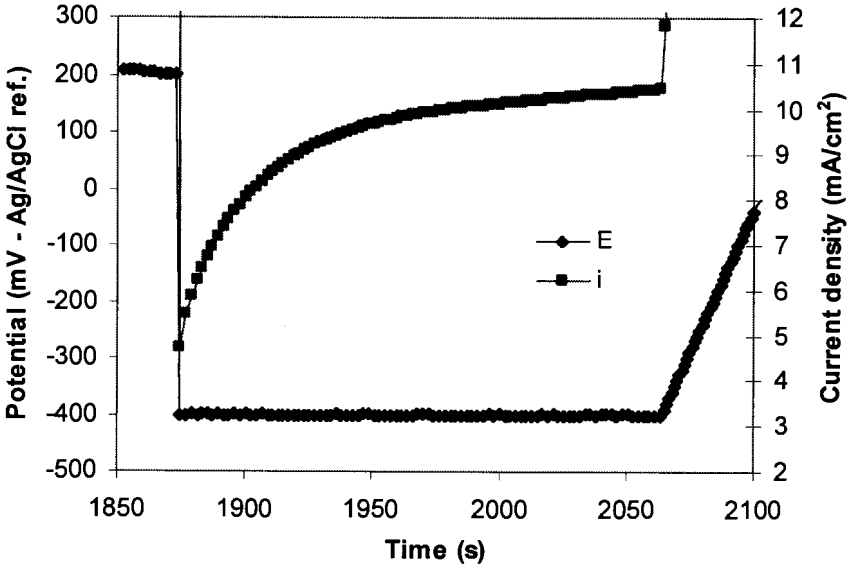

Figure 3-18:Dissolution of salt film in artificial pit experiment – 4 V alloy

Figures 3-16 to 3-18 indicate, as was found for all the alloys, that for the molybdenum containing alloys the salt film dissolved very quickly. Performing artificial pit experiments using 1 mm wire of type 304L Stainless steel and a high purity Fe-19Cr-10Ni alloy Newman and Isaacs [32] found that the salt film present during diffusion controlled dissolution in 0.85 mm deep pits dissolved in about 1 second when the potentiostat is switched off. In the current work, the salt film for the base alloy took substantially longer to dissolve while that for the vanadium alloys showed further increases in dissolution time with increases in vanadium content.

Steinsmo and Isaacs found evidence of slowly dissolving salt film remnants while performing artificial pit tests on 17.4% chromium ferritic stainless steel [51]. They determined the current – concentration relation for different pit depths. After taking solution resistance and diffusion effects into consideration they still found a depth dependence where there should have been none. They proposed that the salt film produces a compound that needs substantially longer times in the active dissolution region before its effect on limiting the active dissolution rate will disappear. It is believed that such a remnant film could have important consequences on the stability of small pits [52]. It was stated that although the salt film dissolves within a second, the effect of the salt film remnants take around 140 seconds to disappear for the 17.4 % Cr ferritic stainless steel. The concentrated solution in the pit could be lost fairly quickly through diffusion while the production rate of corrosion products is limited by this remnant film – causing the concentration to drop below the critical value, thus leading to repassivation.

It is believed that the key to the mechanism for vanadium could lie in the rate of dissolution of the salt film or remnants thereof. If the vanadium changes the dissolution kinetics of this film to a great enough extent, it could lead to the termination of metastable pits when the cover ruptures. In line with the suggestion of Steinsmo and Isaacs, it is proposed that when the cover over the pit is lost and the dissolution of the salt film remnants is very slow, that the pit electrolyte is lost through diffusion by the time the salt film remnants have dissolved, causing the pit to repassivate.

4. Conclusions

Vanadium as alloying element in 18%Cr ferritic stainless steels has as strong an effect in shifting the pitting potential to more anodic values as molybdenum, up to a 4% level of addition. There is however a difference in the mechanism for these two alloy elements. The experimental results confirm the idea that molybdenum lowers the active current density within metastable pits, thereby shifting the potential where a metastable pit reaches the critical stability product to more anodic values. In contrast, vanadium appears to affect the response of the salt film when the diffusion barrier of the metastably growing pit is lowered; the experimental evidence indicates that vanadium decreases the rate of dissolution of the salt film remnants, thereby increasing the probability of repassivation of metastable pits due to loss of the aggressive pit anolyte.

5. References

[1] Metals Handbook 3, "Properties and Selection: Stainless Steels, Tool Materials and Special-Purpose Metals", ASM, pp 17-65, 1980
[2] N.J.E. Dowling, Y.-H. Kim, S.-K. Ahn and Y.-D. Lee, Corrosion 55, No 2, pp 187-199, 1999
[3] D.A. Jones, "Principles and Prevention of Corrosion", second edition, Prentice Hall, USA , p 210, 1992
[4] J.R. Galvele, Treatise on Material Science and Technology 23, ed. J.C. Scully, Academic Press, p1, 1983
[5] J.C. Bavay, Stainless Steels, ed. P. Lacombe, B. Baroux, G. Beranger, Les editions de physique, pp 537-547, 1993
[6] "Corrosion Mechanics in Theory and Practice", ed. P. Marcus and J. Oudar, Chapter 9, B. Baroux, "Further Insights on the Pitting Corrosion of Stainless Steel", Marcel Dekker Inc., New York, p 265, 1995
[7] E. Alfonsson and R. Qvarfort, Materials Science Forum 111-112, pp 483-492, 1992
[8] J.W. Oldfield, International Materials Reviews 32, No 3, pp 153-170, 1987
[9] A.P. Bond, E.A. Lizlovs, H.J. Dundas and A. Poznansky, Electrochemical techniques for corrosion, NACE Corrosion/85, Boston, pp 127-132, 1985
[10] D.E. Williams, J.S. Stewart and P.H. Balkwill, Corros. Sci. 36, No. 7, pp 1213-1235, 1994
[11] R.J. Brigham and E.W. Tozer, J. Eletrochem. Soc. 121, pp 1192-1193, 1974
[12] E.A. Lizlovs and A.P. Bond, J. Electrochem. Soc. 116, No. 5, pp 574-579, 1969
[13] E.A. Lizlovs and A.P. Bond, J. Electrochem. Soc. 122, No. 6, pp 719-722, 1975
[14] E.A. Lizlovs and A.P. Bond, Corrosion (Houston) 31, pp 219-222, 1975
[15] R.D. Knutsen and A. Ball, Corrosion 47, No. 5, pp 359-368, 1991
[16] H.S. Isaacs and R.C. Newman, Corrosion chemistry within pits, crevices and cracks, Ed. A. Turnbull, National Physical Laboratory, HMSO, London, pp 45-59, 1987
[17] H.S. Isaacs and Y. Ishikawa, J. Electrochem. Soc. 132, No. 6, pp 1288-1293, 1985
[18] G.T. Burstein, G.O. Ilevbare, C. Lui, R.M. Souto and S.P. Vines, 14th International Corrosion Congress, Cape Town, 1999. Published on CD-ROM
[19] J.R. Galvele, J. Electrochem. Soc. 123, No. 4, pp 464-474, 1976
[20] P.C. Pistorius and G.T. Burstein, Phil. Trans. R. Soc. Lond. A 341, pp531-559, 1992
[21] H.S. Isaacs and G. Kissel, J. Electrochem. Soc. 119, No. 11, pp 1628-1632, 1972
[22] H.S. Isaacs, J. Electrochem. Soc. 120, No. 11, pp 1456-1462, 1973
[23] P.C. Pistorius and G.T. Burstein, Corros. Sci. 33, No. 12, pp 1885-1897, 1992
[24] J.W. Tester and H.S. Isaacs, J. Electrochem. Soc. 122, No. 11, pp1438-1445, 1975
[25] R.C. Newman and E.M. Franz, Corrosion-NACE 40, No. 7, pp 325-330, 1984
[26] P.C. Pistorius and G.T. Burstein, Corros. Sci. 36, No. 3, pp 525-538, 1994
[27] J.R. Galvele, J.B. Lumsden and R.W. Staehle, J. Electrochem. Soc. 125, No 8, pp 1204-1208, 1978
[28] N. Suutala and M. Kurkela, Proc. Stainless Steel – 84, Gothenburg, pp 240-247, 1984
[29] I. Olefjord and B-O. Elfstrom, Corrosion-NACE 38, No. 1, pp 46-52, 1982
[30] R.C. Newman and E.M. Franz, J. Electrochem. Soc. 131, No. 1, pp 223-225, 1984
[31] R.C. Newman, Corros. Sci. 25, No 5, pp 331-339, 1985
[32] R.C. Newman, Corros. Sci. 25, No 5, pp 341-350, 1985
[33] R.C. Newman and H.S. Isaacs, J. Electrochem. Soc. 130, No. 7, pp 1621-1624, 1983
[34] H.S. Isaacs and M. Kaneko, 14th International Corrosion Congress, Cape Town, South Africa, 1999
[35] N.J. Laycock and R.C. Newman, Corros. Sci. 39, No. 10-11, pp. 1771-1790, 1997
[36] N.J. Laycock, M.H. Moayed and R.C. Newman, J. Electrochem. Soc. 145, No. 8, pp 2622 – 2628, 1998
[37] R.C. Newman, 14th International Corrosion Congress, Cape Town, South Africa, 1999
[38] K. Sugimoto and Y. Sawada, Corrosion-NACE 32, No. 9, pp 347-352, 1976
[39] J.N. Wanklyn, Corros. Sci. 21, No. 3, pp 211-225, 1981
[40] R. Qvarfort, Corros. Sci. 40, No. 2-3, pp. 215-223, 1998
[41] R.D. Davies and F.P.A. Robinson, Corrosion Engineering, NACE, pp 336-340, 1989
[42] H.C. Brookes and F.J. Graham, Corrosion 45, No. 4, pp 287-293, 1989
[43] R. Goetz, J. Laurent and D. Landolt, Corros. Sci. 25, No. 12, pp 1115-1126, 1985
[44] S.C. Tjong, ISIJ International 31, No. 7, pp 738-743, 1991
[45] K. Premachandra and R. Paton, Innovation Stainless Steel, Italy, pp 3.111-3.119, 1993
[46] P.V. Scheers and R. Paton, Corrosion and Prevention 95, Paper 35, 1995

[47] R. Paton, P.V. Scheers and K. Premachandra, Proc. Int. Cong. 'Stainless steels '96', Dusseldorf, Germany, German Iron and Steel Institute, pp 35-40, 1996
[48] R. Paton, Ironmaking and Steelmaking 24, No. 6, pp 441-446, 1997
[49] R. Qvarfort, Corros. Sci. 28, pp. 135-140, 1988
[50] D.E. Williams, C. Westcott and M. Fleischmann, in Corrosion Chemistry within Pits, Crevices and Cracks (ed. A. Turnbull), HMSO, London, pp. 61-87, 1987
[51] U. Steinsmo and H.S. Isaacs, J. Electrochem. Soc. 140, No. 3, pp. 643-653, 1993
[52] U. Steinsmo and H.S. Isaacs, Corros. Sci. 35, Nos 1-4, pp. 83-88, 1993

Appendix A: Experimental alloys

Table A-1: Chemical analyses of experimental alloys

Alloy	Elements (wt%)										
	Cr	Mo	V	C	N	Si	Ni	Mn	Fe	S	P
B	17.7	0.025	< 0.00	0.021	0.023	0.53	0.016	0.53	81.2	0.013	0.02
1 V	18.1	0.030	0.89	0.022	0.022	0.50	0.010	0.54	79.7	0.014	0.02
2 V	18.0	0.030	1.88	0.024	0.023	0.42	0.010	0.51	79.0	0.010	0.02
4 V	18.0	0.030	3.77	0.027	0.025	0.40	0.010	0.54	79.4	0.010	0.02
1 Mo	18.0	0.920	0.10	0.021	0.025	0.55	0.010	0.51	79.8	0.014	0.02
2 Mo	18.0	1.930	0.009	0.020	0.021	0.55	0.010	0.51	78.8	0.014	0.03
4 Mo	17.7	3.800	0.009	0.023	0.021	0.56	0.010	0.52	77.6	0.015	0.02

Tables A-2 (a,b): SEM-EDS analyses of precipitates in 4 Mo alloy

(a)

Element	Atom%	Wt%
Si	0.90	0.45
Cr	42.03	39.04
Mn	0.82	0.81
Fe	51.25	51.13
Mo	5.00	8.57

(b)

Element	Atom%	Wt%
Si	0.85	0.43
Cr	43.11	40.23
Mn	0.60	0.60
Fe	50.98	51.09
Mo	4.45	7.66

Table A-3: SEM-EDS analyses of precipitates in 4 V alloy

Element	Atom%	Wt%
Si	0.68	0.37
Cr	10.37	10.48
Mn	0.11	0.12
Fe	11.77	12.77
V	76.92	76.16

Appendix B: Experimental polarisation diagrams

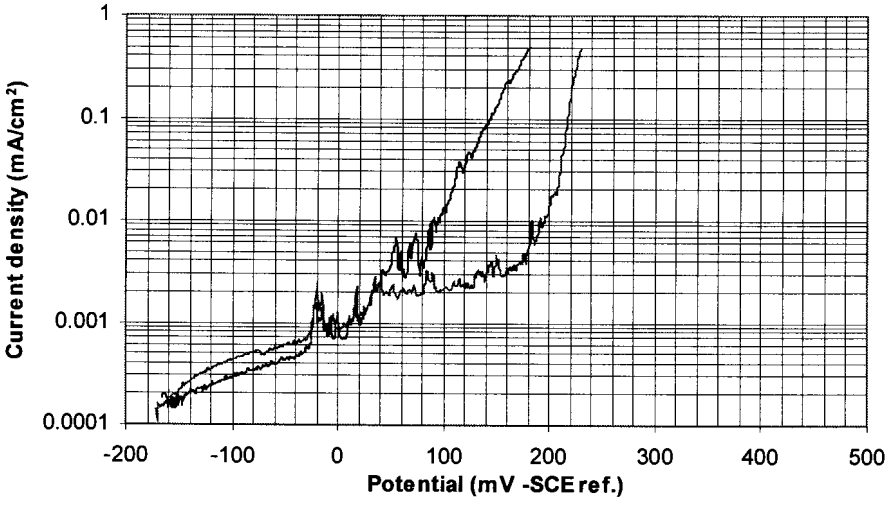

Figure B –1: Polarisation curves for base alloy

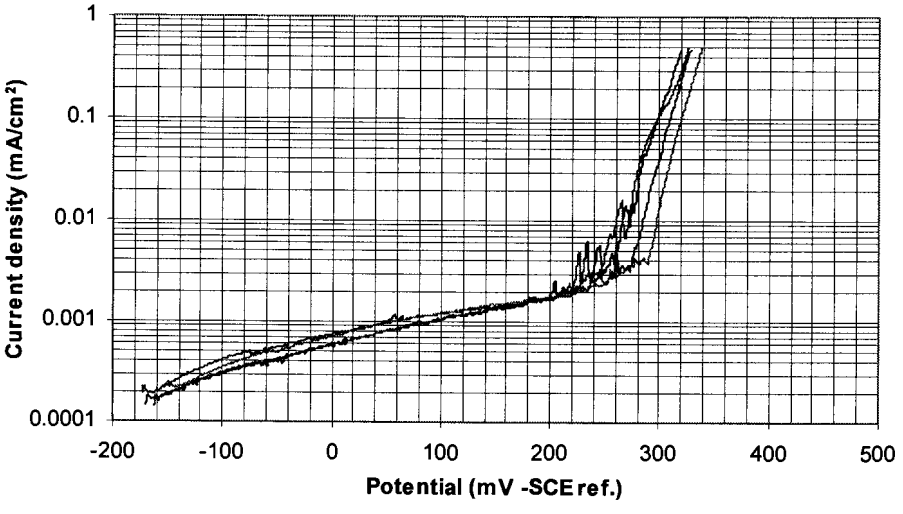

Figure B–2: Polarisation curves for 1 Mo alloy

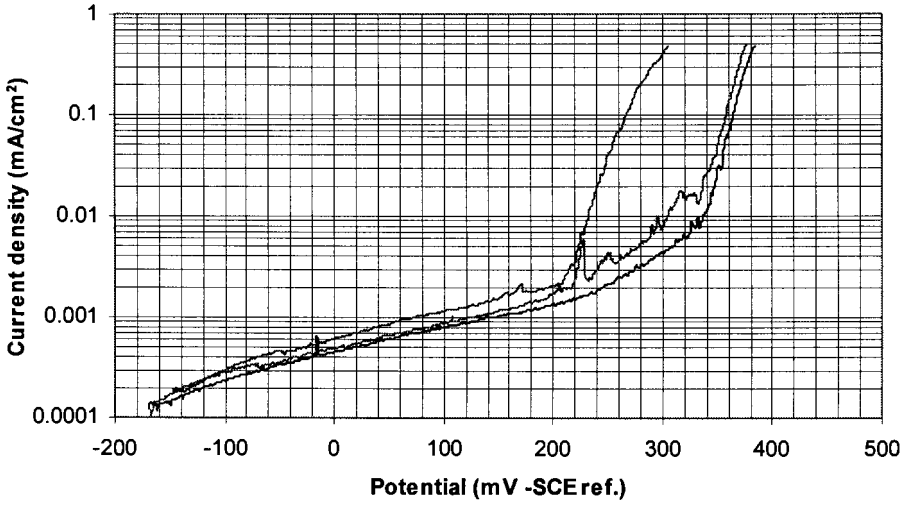

Figure B–3: Polarisation curves for 2 Mo alloy

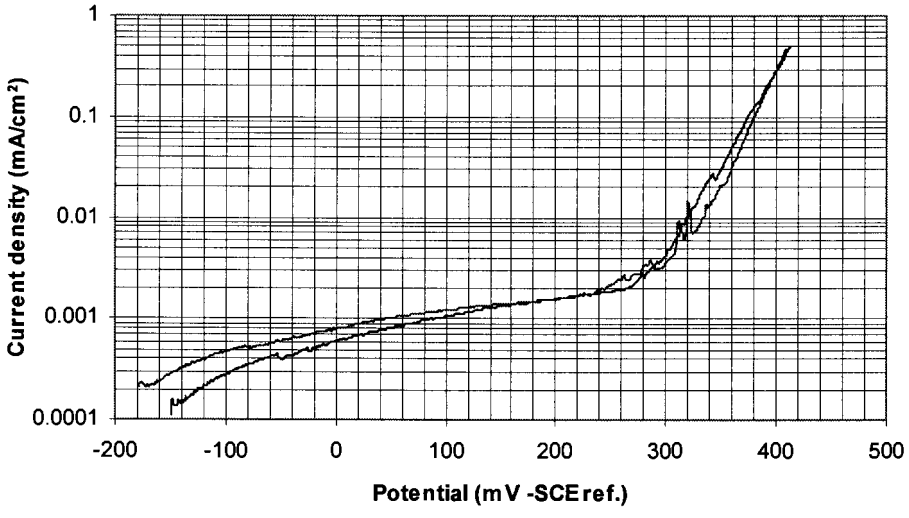

Figure B–4: Polarisation curves for 4 Mo alloy

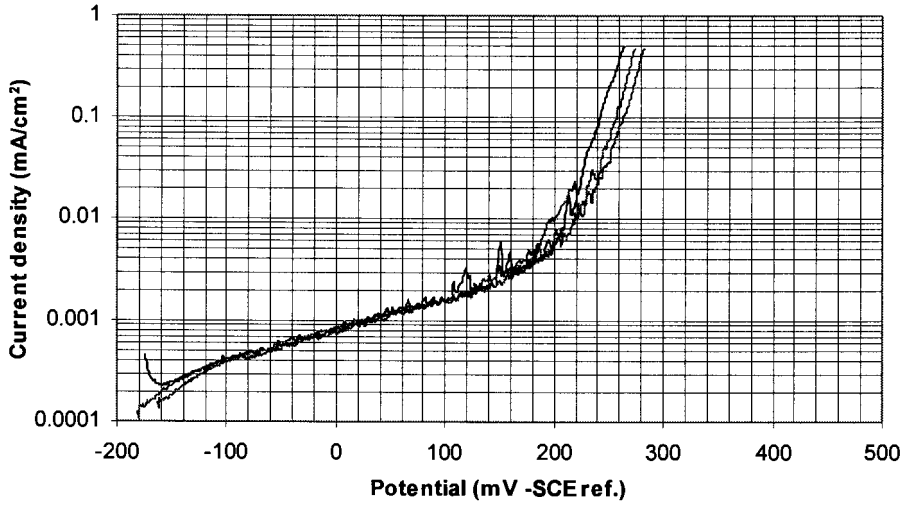

Figure B–5: Polarisation curves for 1 V alloy

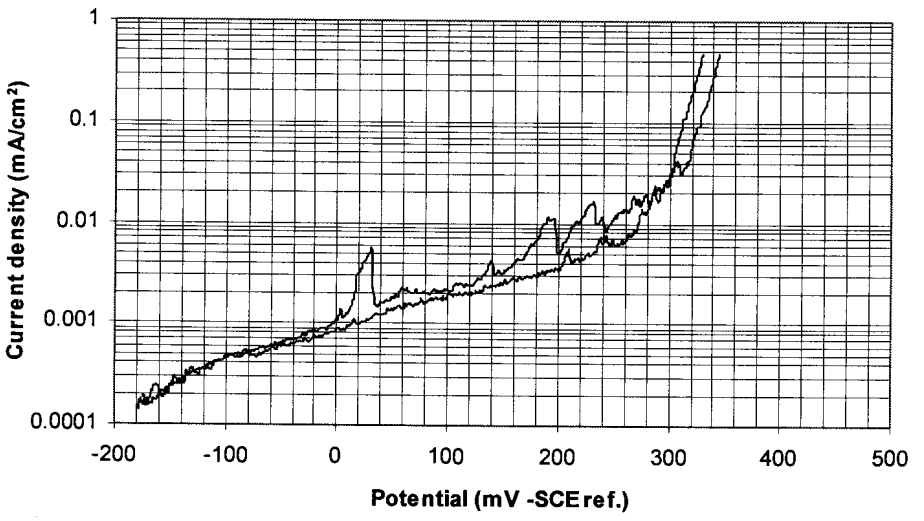

Figure B–6: Polarisation curves for 2 V alloy

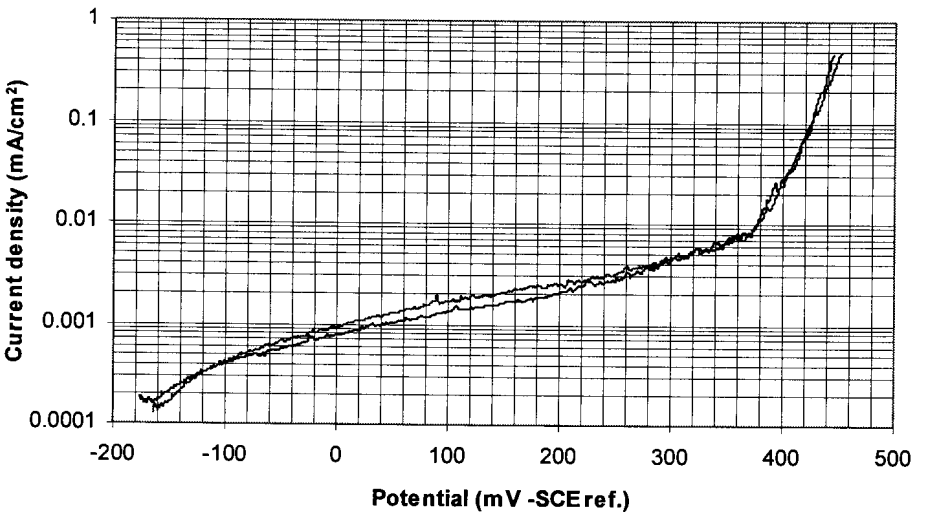

Figure B–7: Polarisation curves for 4 V alloy

Appendix C: Charge calculations for artificial pit tests

The pits were grown by controlling the potential and measuring the amount of charge that flowed. The amount of charge that should flow to create a 0.5 mm deep pit were determined by assuming that the alloys consists only of 18% Cr and 82% Fe with Fe going to Fe^{2+} and Cr going to Cr^{3+}. The density of the alloys was taken as 7.74 g/cm^3.

Calculations:

Volume of pit:	V	$= 0.5 \times 0.5 \times 0.5$
		$= 0.125$ mm^3
Mass of metal to dissolve:	m	$= 0.125 \times 7.74 \times 10^{-3}$
		$= 0.967 \times 10^{-3}$ g
Mass of Fe to dissolve:	m_{Fe}	$= 0.793$ mg
Mass of Cr to dissolve:	m_{Cr}	$= 0.174$ mg
Moles Fe to dissolve:	n_{Fe}	$= 1.42 \times 10^{-5}$ gmol
Moles Cr to dissolve:	n_{Cr}	$= 0.335 \times 10^{-5}$ gmol
Number of electrons transferred:	N_e	$= (2n_{Fe} + 3n_{Cr}) \times 6.022 \times 10^{23}$
		$= 2.32 \times 10^{19}$
Charge passed: Q		$= N_e \times 1.602 \times 10^{-19}$
		$= 3.71$ C

Appendix D: Additional Artificial pit results

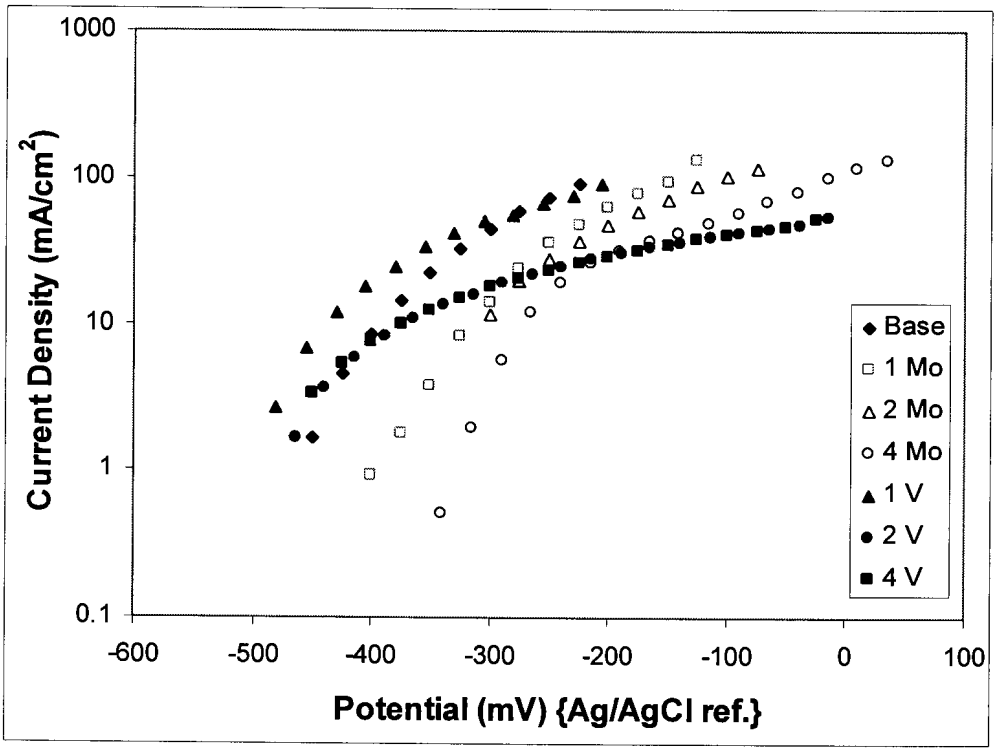

Figure: D-1: Measured polarisation data for artificial pits (second set)

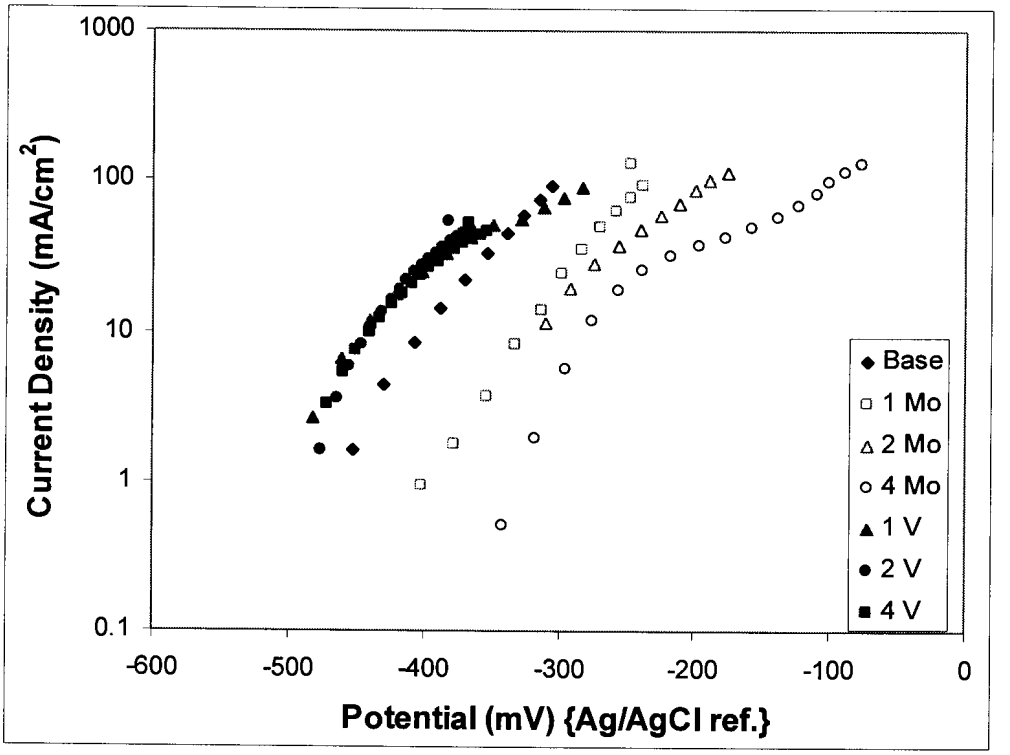

Figure: D-2: Measured polarisation data for artificial pits – IR adjusted (second set)

Appendix E: Examples of metastable pits formed during small electrode experiments

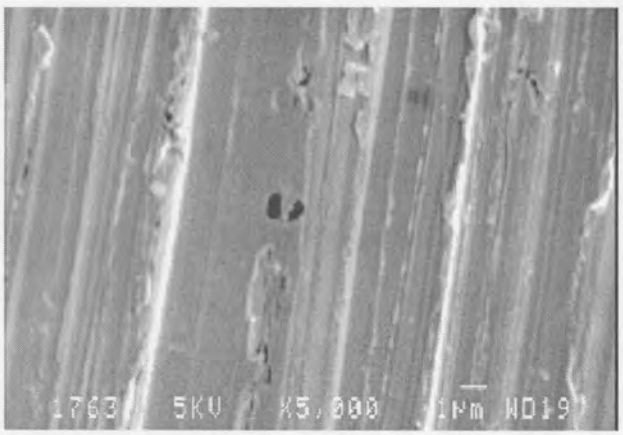

Figure E–1: Small partially covered pit in base alloy

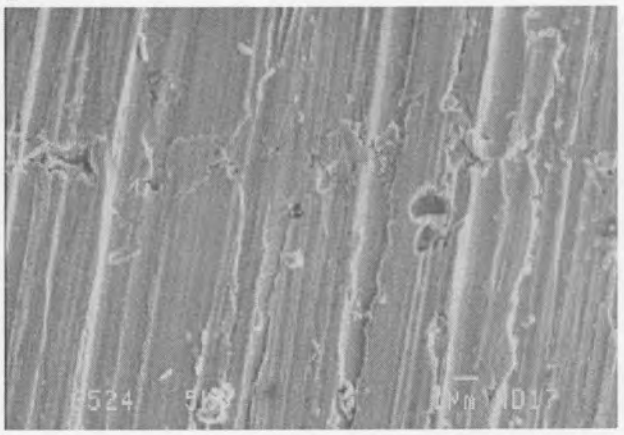

Figure E–2:Small open pit in base alloy

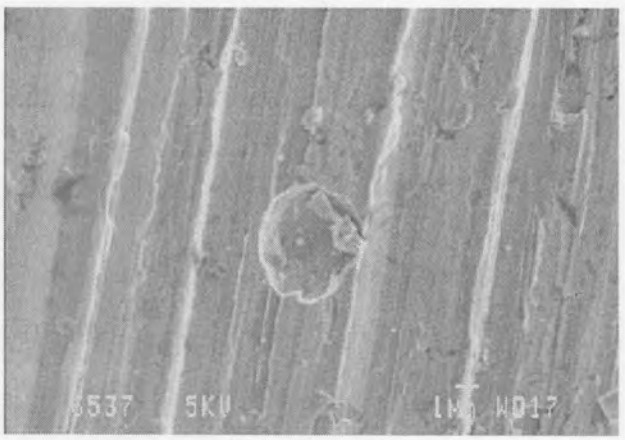

Figure E–3: Open pit in 2 V alloy

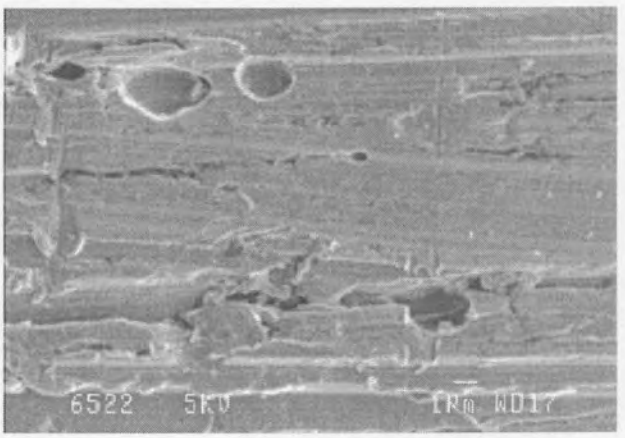

Figure E–4: Open pits fairly close together in base alloy

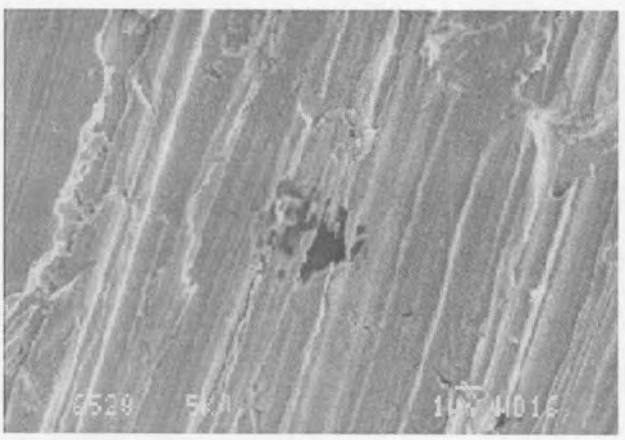

Figure E-5: Pit in 4 Mo alloy showing remains of cover

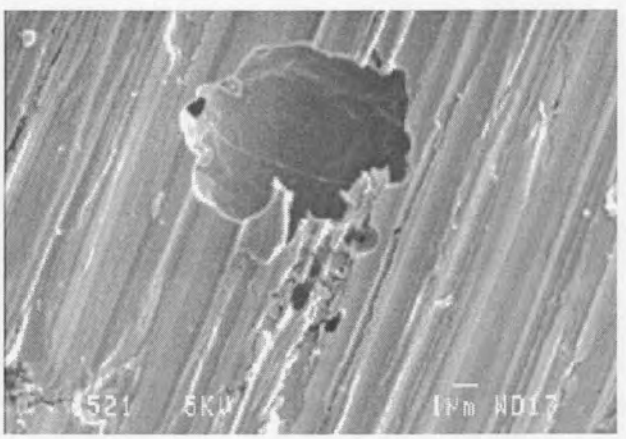

Figure E–6: Large open pit in 1 Mo alloy showing remains of cover

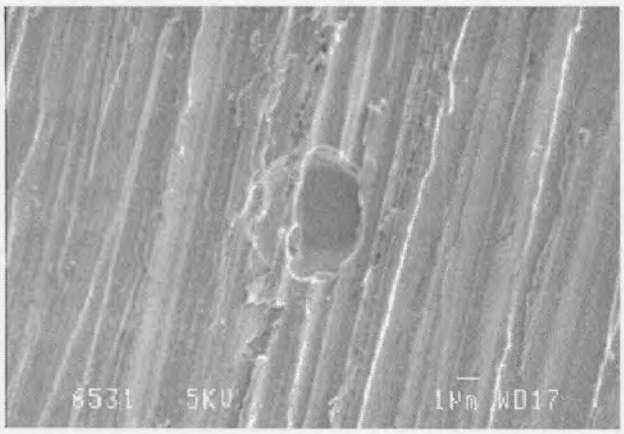

Figure E-7: Open pit in 4 V alloy with a strand of passive film still intact over mouth

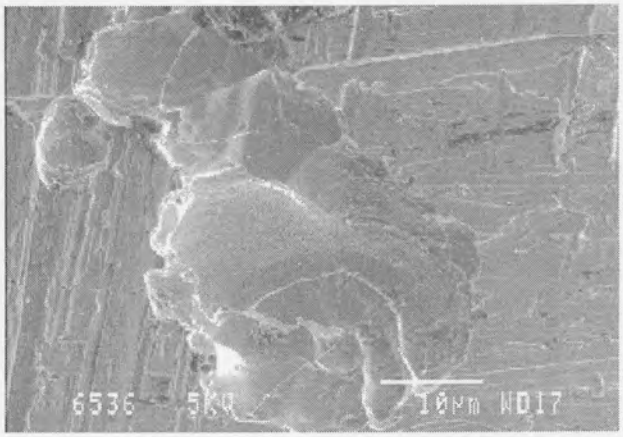

Figure E–8: Large open pit in 2 V alloy

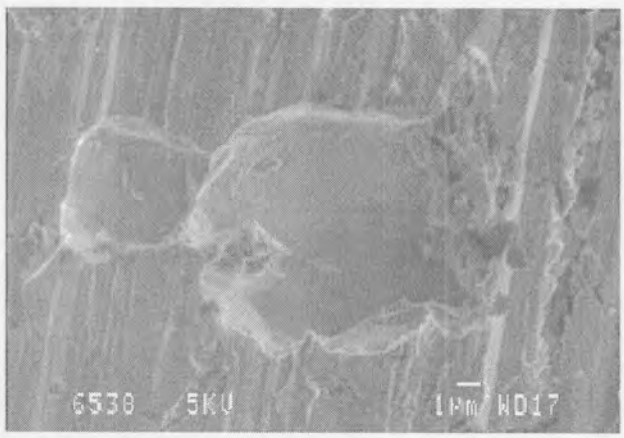

Figure E–9: Large open pits in 2 V alloy

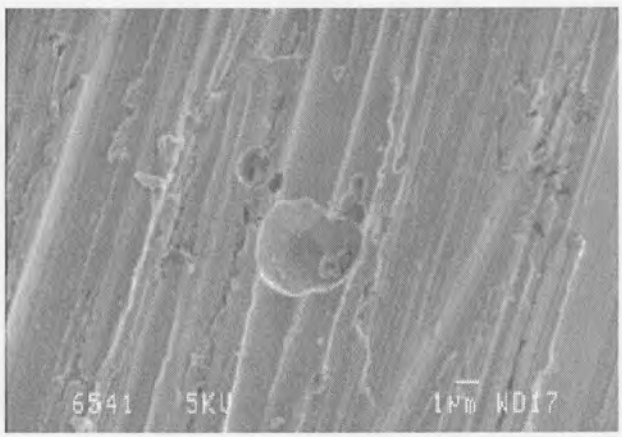

Figure E–10: Open pit in 1 V alloy

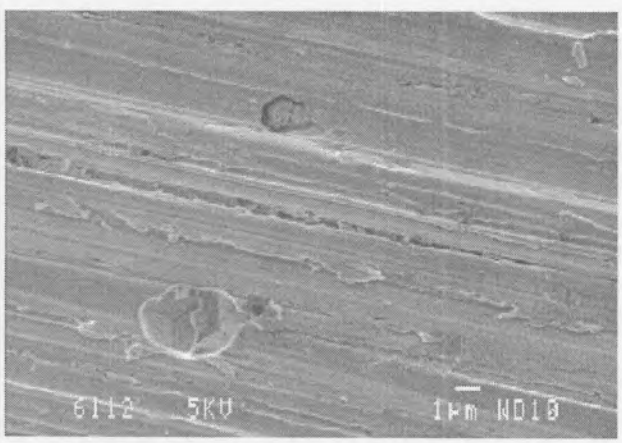

Figure E-11: Open pit in base alloy

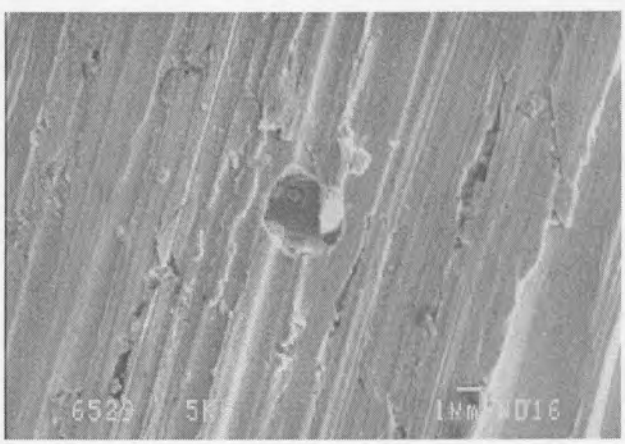

Figure E-12: Open pit in 4 Mo alloy

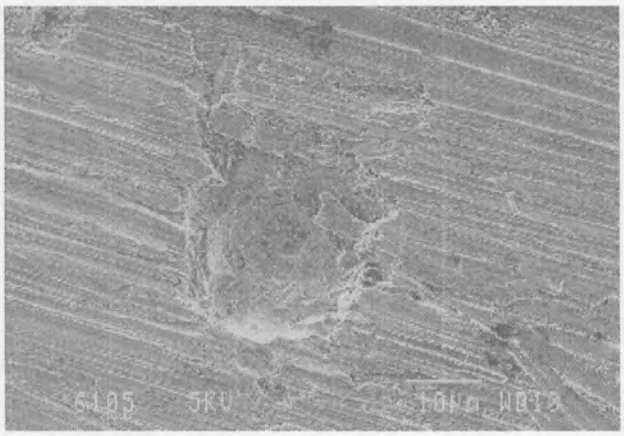

Figure E-13: Open pit in 1 V alloy

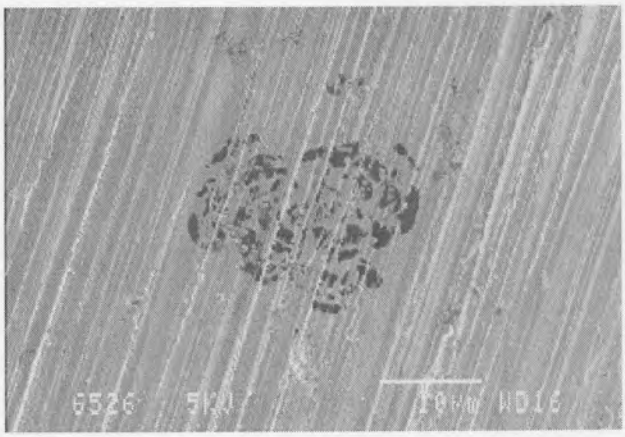

Figure E-14: Partially covered pit in 4 Mo alloy

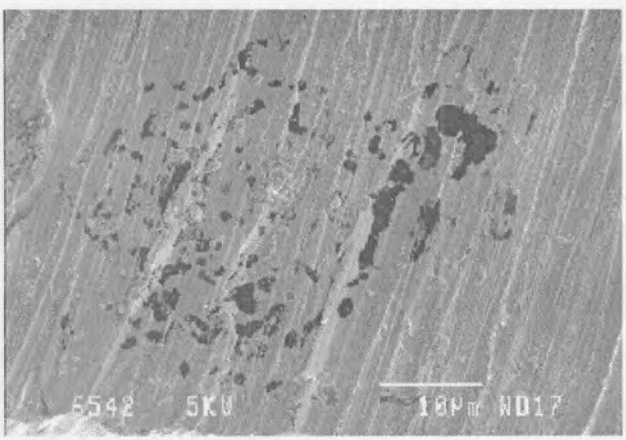

Figure E-15: Partially covered pit in 1 V alloy

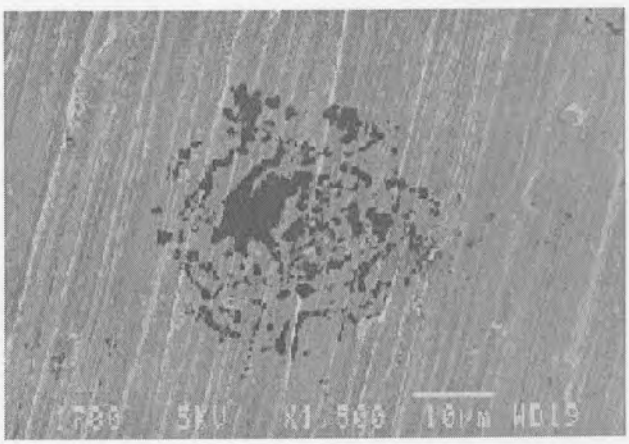

Figure E-16: Partially covered pit in 4 Mo